Acta Geotechnica (2024) 19:741–762
https://doi.org/10.1007/s11440-023-01961-x

RESEARCH PAPER

# Mechanical and microstructure analysis of mass-stabilized organic clay thermally cured using a ternary binder

Victor Núñez[1] · Andres Lotero[1] · Cezar Augusto Bastos[2] · Paul Sargent[3] · Nilo Cesar Consoli[1]

Received: 20 October 2022 / Accepted: 2 June 2023 / Published online: 24 June 2023


## Abstract

The technique of mass soil stabilization using alternative binders to Portland cement (PC) has been used successfully in the past. However, knowledge gaps exist regarding the design of these binders. Ground-granulated blast furnace slag (GGBS) has been widely used as a substitute for PC; however, it requires an alkaline activator (e.g. lime and PC) to promote pozzolanic reaction and strength enhancement. A candidate that presents a less energy-intensive manufacturing and carbon footprint is carbide lime (CL), a by-product of acetylene gas production, rich in $Ca(OH)_2$. The main problem with the pozzolanic binder in the stabilization technique is its slow reaction kinetics and the long time required for laboratory-scale investigations before in situ application. Therefore, this research presents a dosing study of a ternary binder (TB) comprising CL, GGBS and PC type III (CEM-III) to mass-stabilize a clayey organic soil using thermal curing as an innovative technique to improve the feasibility of laboratory-scale investigations. The effects of binder composition and thermal curing time on the evolution of strength, stiffness, mineralogy, and microstructure were determined. The results, supported by a statistical analysis (ANOVA) and by a multivariate regression analysis (MRA), have shown that the new TB produced a superior mechanical response to soil samples stabilized exclusively with CEM-III. This was evidenced by a less porous microstructure (more reaction products) and mainly the formation of a C–A–S–H gel, as a product of CEM-III hydration and alkaline activation of GGBS (blended cement), whereby the CL content played a key role for the development of the long-term pozzolanic reaction.

**Keywords** Carbide lime · Ground-granulated blast furnace slag · Mass stabilization · Organic clayey soil · Thermal curing

✉ Andres Lotero
andreslotero@hotmail.com

Victor Núñez
vferreiranunez@gmail.com

Cezar Augusto Bastos
cezarbastos@furg.br

Paul Sargent
p.sargent@ulster.ac.uk

Nilo Cesar Consoli
consoli@ufrgs.br

[1] Graduate Program in Civil Engineering, Universidade Federal do Rio Grande do Sul, Porto Alegre, RS 90035-190, Brazil

[2] Universidade Federal do Rio Grande, Rio Grande, RS 96203-295, Brazil

[3] Belfast School of Architecture and the Built Environment, Ulster University, Belfast BT15 1ED, Northern Ireland, UK

## 1 Introduction

Due to ever-increasing rates of urbanization worldwide, this has led to new construction on greenfield sites in areas such as alluvial floodplains that are underlain by problematic soils, such as highly compressible organic clays. To facilitate construction on sites characterized by such challenging ground conditions, ground improvement is required. Whilst there are a wide range of commercially available ground improvement techniques, one of the most popular techniques for treating soft clays is mass stabilization. This technique was developed in Finland during the early 1990's, whereby the first large-scale applications were undertaken in 1993 on sites underlain by peat to facilitate the construction of highway and railway infrastructure network in Finland and Sweden. Peat soils were

treated with conventional cementitious agents (mainly PC and lime) up to a maximum depth of 5–6 m [5, 59, 88].

As the stabilized mixture presents disponible water during the curing process, a moulding methodology was developed that aims to simulate site conditions for mass stabilization in the laboratory, which has since been adopted by numerous authors [6, 9, 59, 83]. In general, this technique consists in mixing the binder with the soil and then inserting this mixture into cylindrical moulds with a permeable material (e. g. geotextile) at its base. The specimens are cured partially immersed in water using a preload of 18 kPa to represent 1.0 m landfill composed by granular material [54, 59].

On the other hand, in response to the global climate emergency and the need to decarbonize the construction industry, geotechnical and concrete/cement practitioners alike are focused on the development of new low-carbon alternative binder systems to traditional agents such as PC and lime. These materials are responsible for producing up to 10% of the world's anthropogenic carbon dioxide emissions, due to the energy-intensive processes involved in their manufacture [2, 58, 101]. Hence, this serves as a motivating factor to investigate new types or families of cementitious agents, and especially binders that can be produced from alternative, low value-added materials and have longevity in supply.

The most popular category of materials for developing as cementitious binders are industrial wastes and by-products containing aluminosilicates in vitreous phases, i.e. with pozzolanic properties. Some examples of these materials are pulverized fly ash (PFA), GGBS, rice husk ash, ground ceramic and glass waste, among others [46, 47, 65, 85, 119]. This negates the need to use high-cost energy-intensive processes to explore/exploit raw (geological) materials, and has the added value of enhancing the circular economy and valorizing high-volume wastes. Mass soil stabilization using alternative waste-based binders also aims to reduce project costs and improve environmental credentials [59, 83, 86, 123].

Numerous studies have successfully demonstrated that binders based on these residues can improve the performance of stabilized soils, especially for long curing times [45, 48, 105, 110]. However, there is a lack of research concerning the optimization of the dosage of these cementitious mixtures for mass soil stabilization applications [76, 125]. Furthermore, one of the challenges associated with the development of new low-carbon alternative waste-based binders is their slow rate of pozzolanic reactions. This, in turn, makes initial laboratory investigations of binder designs and dosages to achieve strength requirements (as recommended by EuroSoilStab [54]; Kitazume and Terashi [78]; Forsman et al. [59] prior to on-site implementation) impractical, considering the large execution time demanded by such studies. On the other hand, Ahnberg et al. [6] reported that short-term strengths can be reliably obtained when using OPC-based binders, thereby justifying its inclusion (partially) when rapid hardening development is required in mass soil stabilization.

GGBS is a by-product of iron production that, in addition to having significant aluminosilicate content in reactive phases, can also have latent or potential hydraulic capacity, i.e. when finely ground and mixed with water, it can set and harden [62, 95, 96]. GGBS has been widely used in laboratory- and field-scale soil stabilization, allowing acceptable engineering performances [1, 32, 55, 65]. However, when GGBS is used alone it possesses a slow hydration rate—resulting in very slow and low strength gains [31]. Therefore, GGBS requires alkali activation to promote the dissolution of existing aluminosilicate chains within the GGBS, which releases $OH^-$ ions and accelerates hydration and pozzolanic reactions [90, 93]. This can be achieved through the addition of agents such as lime (hydrated or quicklime) or even through the portlandite content resulting from the OPC hydration reactions [32, 68]. This in turn enables the formation of new cementitious gels [113]. When the GGBS hydrates and reacts with these alkaline agents, it commonly produces gels such as calcium–silicate–hydrates (C–S–H) and calcium–alumina–hydrates (C–A–H) [93]. Although the mixing of GGBS with industrial limes (CaO or $Ca(OH)_2$) for mass soil stabilization has been addressed in previous work, information regarding the influence of the dosage of this cementitious mixture on the performance of the stabilized soil is very limited [3, 6, 54, 72].

Similarly, carbide lime (CL) is a by-product (low value-added) of acetylene gas production, which has good affinity for aluminosilicates and has previously been reported to promote pozzolanic reactions [116]. This is due to the characteristic composition of this by-product (high portlandite content) [47, 49]. Consequently, this therefore highlights the potential of converting CL from a waste to a possible valuable engineering material for incorporation within alkali-activated cementitious materials (AACMs) for soil stabilization applications [25, 40, 43, 45–47, 85, 103, 107]. Previous studies have evaluated the use of CL as an activator to GGBS [82, 108, 124]; however, none have investigated its use in the mass soil stabilization method.

This study aims to improve the state-of-the-art of alternative binders in mass soil stabilization, by investigating the technical prospects of a new ternary binder (TB) comprising CL, GGBS and Type III-PC (i.e. CEM-III) for stabilizing a soft organic clayey soil. This binder design was selected to achieve initial high strength gains induced by CEM-III, and long-term high strength development

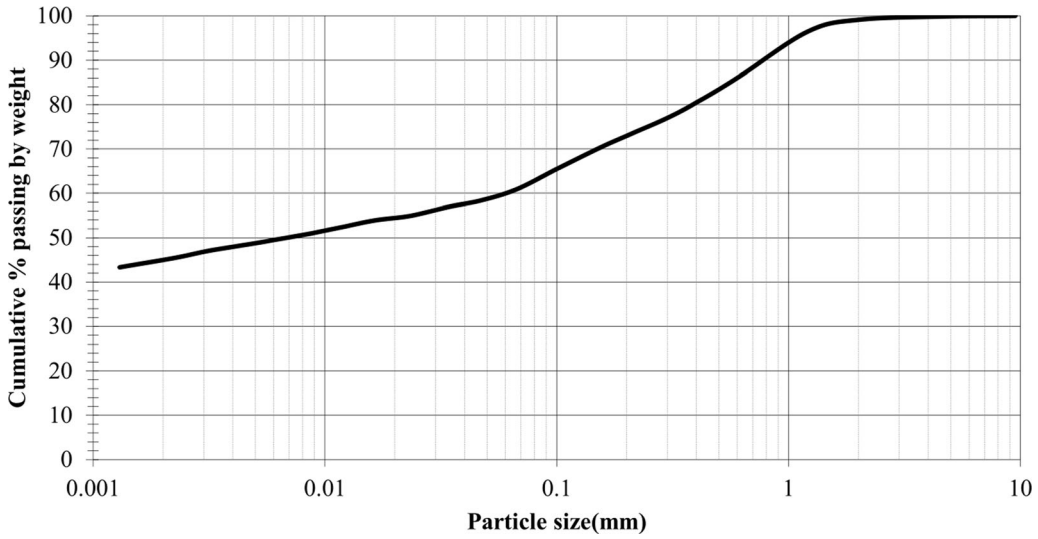


**Fig. 1** Grain size distribution of organic clayey soil

**Table 1** Physical properties of the soil under study

| Properties | Organic Clay Soil | References/method |
|---|---|---|
| Specific gravity (g/cm$^3$) | 2.43 | [9] |
| Clay (diameter < 0.005 mm) | 48% | [12] |
| Silt (0.002 mm < diameter < 0.075 mm) | 14% | [12] |
| Sand (0.075 mm < diameter < 4.75 mm) | 37% | [13] |
| Gravel (4.75 mm < diameter < 60 mm) | 1% | [13] |
| Site moisture content | 40% | [16] |
| Liquid limit ($w_L$) | 71% | [15] |
| Liquid limit ($w_L$ dried 100 °C) | 49% | [15] |
| Plastic limit ($w_P$) | 40% | [15] |
| Plastic index ($PI$) | 31% | [15] |
| Organic matter content | 10.5% | [19] |
| Organic soil classification | Medium-organic soil | [75] |
| pH (portable pH meter) | 4.5 | [69] |
| pH (laboratory pH meter) | 4.13 | [16] |
| Classification HRB | A-7-5(17)—Clayey soils, very bad behaviour as pavement base | [10] |
| Classification USCS | OH (organic soil—high compressibility) | [11] |

promoted by CL and GGBS pozzolanic reactions. This investigation was carried out using laboratory-scale mass soil stabilization techniques, which also involved the use of thermal curing through custom-built piece of apparatus for this work. This enabled a rapid analysis of future strength development for mass-stabilized soil mixtures, thereby improving the feasibility of the laboratory practices prior to in situ application. This innovative methodology was applied to improve the rate of reactions and subjected to a statistical assessment to obtain reliable insights into correlations between ternary binder dosage, curing time, geomechanical behaviour and physico-chemical properties.

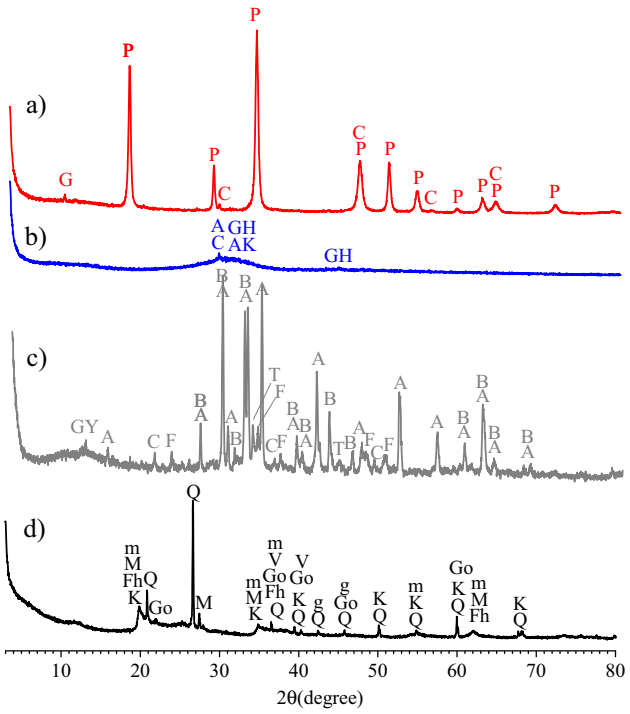


**Fig. 2** XRD spectra for: **a** carbide lime ('CL'), **b** ground-granulated blast furnace slag ('GGBS'), **c** Type 3 Portland cement ('CEM-III') and **d** organic clayey soil ('SOIL'). A: Alite-C3S (tricalcium silicate); AK: akermanite; B: belite-C2S (dicalcium silicate); C: calcite; E: ettringite; F: C4AF (tetracalcium aluminoferrite); Fh: ferrihydrite; G: graphite; Go: goethite; Gy: gypsum; GH: gehlenite; g: gibbsite; K: kaolinite; m: muscovite; M: Montmorillonite; P: portlandite; Q: quartz; T: C3A (tricalcium aluminate)

## 2 Materials and methods

### 2.1 Materials

#### 2.1.1 Soil

The soil of interest for mass stabilization in this study was an organic clay obtained from Pelotas, in southern Brazil. The sampling site was situated in the Santa Bárbara River basin, which is characterized by low-lying topography. During periods of heavy rainfall, the site is prone to flooding and results in swamp-like conditions. The particle size distribution curve for the soil is presented in Fig. 1, with other index properties reported in Table 1. The soil can be classified as a medium organic, black, plastic, sandy clay with an acid pH [16]. According to the Unified Soil Classification System [11], the soil is an organic highly compressible soil (OH). The soil's low pH can be associated with its high cation exchange capacity, which is an influential physico-chemical property that dictates the success of the soil stabilization process [29].

The mineralogical composition of the soil was determined through X-ray diffraction (XRD), whereby the apparatus used was a D8 ADVANCE Bruker X-ray diffractometer with a scan angle (2θ) from 2° to 80°. Based on the XRD spectra produced for the soil (Fig. 2d), the main mineral phases identified were predominantly quartz, along with other constituents including kaolinite and muscovite.

#### 2.1.2 Binder

A new TB was used for this study, comprising a high early strength Portland cement type III (CEM-III), GGBS and CL. According to standard ASTM C150 [17], CEM-III was used as one component of the TB and for reference purposes. As presented in Fig. 2c, XRD analysis determined that the mineralogy of the CEM-III chiefly comprised alite ($C_3S$) and belite ($C_2S$), along with some other minor constituents including $C_4AF$, $C_3A$, calcite, gypsum, portlandite and quartz. This is in agreement with spectra reported in previous studies [63, 106, 109, 115]. The chemical composition of Portland cement was studied by X-ray fluorescence (Table 2). The results report contents of 58.7% CaO, 20.1% $SiO_2$, 5.3% $Al_2O_3$, 3.0% MgO, 3.1% $Fe_2O_3$ and 2.8% $SO_3$ (with other oxides present in smaller percentages). The findings are in agreement with the average elemental composition of fast-hardening Brazilian PC cited by other authors [7, 36, 66, 87].

The GGBS used in this study was sourced from a blast furnace located near the city of Vitória, in south-eastern Brazil. The particle morphology of the GGBS was akin to a coarse sand. Therefore, to increase the reactivity of the GGBS, it was subjected to milling using a ball mill with subsequent sieving in 45 μm. XRD analysis for the GGBS (as presented in Fig. 2b) indicated the presence of alite, calcite, gehlenite and akermanite (in agreement with previous studies by Seo et al. [108]; Trindade et al. [118] and

**Table 2** Chemical composition by X-ray fluorescence of starting materials for the ternary binder

| Material | $SiO_2$ | $Al_2O_3$ | CaO | MgO | $Fe_2O_3$ | $TiO_2$ | $K_2O$ | $SO_3$ | $Na_2O$ | C |
|---|---|---|---|---|---|---|---|---|---|---|
| CEM-III | 20.1 | 5.3 | 58.7 | 3.0 | 3.1 | 0.1 | 0.2 | 2.8 | ND* | ND* |
| GGBS | 34.3 | 12.1 | 41.0 | 7.5 | 0.2 | 0.7 | 0.4 | 1 | 0.2 | 0.1 |
| CL | 3.1 | 1.9 | 71.6 | 0.6 | 0.9 | 0.1 | ND* | 0.3 | ND* | ND* |

**ND* not detected

Kourti et al. [80]). The GGBS possessed a crystallinity index of 2.1%, which was determined using the amorphous subtraction method proposed by Ruland [100] and widely successfully used [94, 99, 117, 121]. This indicated that the GGBS was characterized by 97.9% of amorphous phases, which comfortably exceeds the minimum amorphous content of 67% required by British standard EN 15167-1 [24] for use as an addition to ordinary Portland cement (CEM-I). The composition of the GGBS was also studied by XRF (Table 2), resulting in a composition of 41.0% CaO, 34.3% $SiO_2$, 12.1% $Al_2O_3$, 7.5% MgO and other elements in very small percentages (trace elements). Its high basicity index ($CaO/SiO_2$ ratio > 1.0) indicates its basic character.

The CL used in this study was obtained near the city of Porto Alegre, in southern Brazil. As a result of the acetylene gas production process, the resulting CL possesses a high-water content, which consequently produces agglomerations of powdered material. Thus, the material was dried for 24 h at 60 °C, followed by manual crushing using a porcelain mortar and pestle, with subsequent sieving using a 75 μm sieve. XRD spectra for the CL (as presented in Fig. 2a) indicates the main presence of portlandite, along with other minority phases including calcite and graphite. This corroborates findings previously made by Thomé [116], Horpibulsuk et al. [70], Vichan and Rachan [120], Saldanha et al. [102] and Lotero et al. [85]. The chemical composition of the CL presented in Table 2 has also been studied by other authors through XRF [27, 85, 102], so the dominant oxide reported was CaO, along with some other minor oxides.

## 2.2 Experimental design

Different parameters were investigated in the study, which were subdivided into 'controllable factors', 'constant factors' and 'response variables'. Table 3 summarizes these parameters, together with their description and the study levels adopted for each variable. In a general way, the experimental plan evaluates the influence, of the percentage of substitution of CEM-III by an alternative fraction (GGBS + CL), and the percentage of CL in each substitution of CEM-III, on the mechanical performance of the soil stabilized with TB. A central composite experimental design (CCD) is proposed to analyse the influence of the linearity and pure quadratic behaviour of the controllable factors, as well as the possible effects of their interaction on the response variables (second-order model). The CCD couples a full factorial design ($2^k$) of three controllable factors ($2^3$). Each controllable factor has low and high levels, which were represented in corners of the cube (Fig. 3), to assess linear effects on the response variables ($q_u$ and $E_{50}$).

A point in the centre of the cube (central level) and six axial points (levels on the cube faces) were also used, thereby forming a star to allow more in-depth

**Table 3** Summary of investigated variables

| Category | | Parameter | Description | Study Level | | |
|---|---|---|---|---|---|---|
| | | | | Low | Central | High |
| Controllable variables | Controllable factors | Percentage substitution of CEM-III (%Substitution) | Per cent of mass of Portland cement was replaced by an alternative fraction, composed by GGBS + CL (e.g. for % substitution of 65 wt%, the ternary binder was composed by 65 wt% of alternative fraction and 35 wt% of CEM-III) | 50 wt% | 65 wt% | 80 wt% |
| | | *CL* content (*%CL*) | Per cent of mass of alternative fraction is composed by CL (e. g. for %CL of 30%, the alternative fraction was composed by 30% of CL and 70% of GGBS) | 30% | 50% | 70% |
| | | Curing time | Time (in days) of specimens thermal curing | 1 day | 7 days | 13 days |
| | Constant factors | Curing condition | Temperature controlled | 60 ± 0.5 °C | | |
| | | Binder content | Percentage of binder with respect to the dry weight of the soil | 200 kg/m$^3$ | | |
| | | Preload | Stabilized soil mixtures were subjected to preloading during curing to accelerate consolidation and densification to produce higher strength gains | 18 kPa | | |
| | | Soil moisture content | Percentage of water in the soil with respect to the dry soil mass | 1.25 times liquid limit ($w_L$) = 87.5% | | |
| Response variables | | Unconfined compressive strength | Maximum compressive stress recorded for cured stabilized soil samples, $q_u$ (kPa) | – | | |
| | | Elastic stiffness | Young's modulus secant measurement, $E_{50}$ (MPa) | – | | |

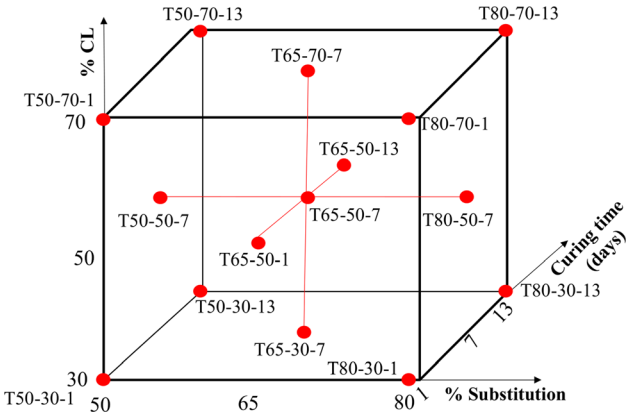


**Fig. 3** Experimental program treatments (central composite design—CCD)

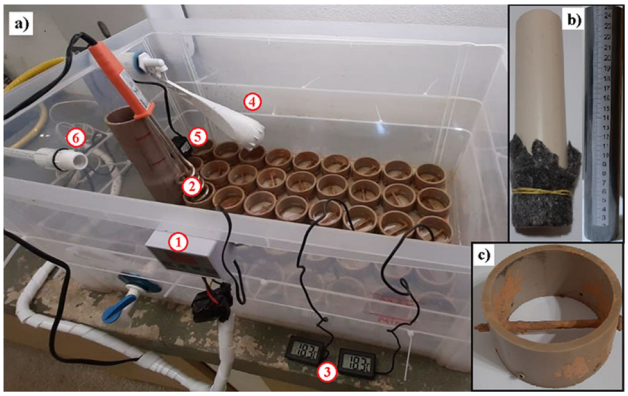


**Fig. 4** Storage container for moulding and curing of lab-scale samples: **a** Automated sample moulding and curing box, where '1' is a thermostat, '2' is a heater, '3' are thermometers, '4' is a float valve, '5' is a water pump and '6' is an overflow pipe; **b** Cylindrical mould and steel cylinder for preload and **c** lower support "cylindrical rings"

investigations regarding the pure square behaviour of these factors [67]. Triplicates were designed for each point of the cube (except for the central point cited—6 replicates), which in turn produced a total of 48 trials for the 15 different points of the cube (experiment treatments). The cube presented in Fig. 3 summarizes the mixtures or treatments of the experimental design. Equations relating the controllable factors to the response variables were defined through a multivariate regression analysis (MRA) in order to verify the possibility of mathematically modelling $q_u$ and $E_{50}$ from the proposed second-order design and thus obtain response surfaces.

The levels adopted for the controllable factors (Table 3) were defined based on reference studies [1, 23, 74, 82, 95, 96, 108] and results of preliminary tests carried out by the authors, taking into account the lack of information on the mass stabilization of the local soil with the wastes under study and the effect of its thermal curing.

**Table 4** Binder design mixtures (or treatments) in the experimental program

| Mixture [T($x$)-($y$)-($z$) or PC($z$)] | Controllable factor level studied | | | Content (wt%) of ternary binder fractions | | |
|---|---|---|---|---|---|---|
| | %Substitution ($x$) | %CL ($y$) | Curing time – days ($z$) | CL (wt%) | GGBS (wt%) | CEM-III (wt%) |
| T50-30-1 | 50 | 30 | 1 | 15 | 35 | 50 |
| T50-70-1 | 50 | 70 | 1 | 35 | 15 | 50 |
| T80-30-1 | 80 | 30 | 1 | 24 | 56 | 20 |
| T80-70-1 | 80 | 70 | 1 | 56 | 24 | 20 |
| T65-50-1 | 65 | 50 | 1 | 32.5 | 32.5 | 35 |
| T50-50-7 | 50 | 50 | 7 | 25 | 25 | 50 |
| T65-30-7 | 65 | 30 | 7 | 19.5 | 45.5 | 35 |
| T65-70-7 | 65 | 70 | 7 | 45.5 | 19.5 | 35 |
| T80-50-7 | 80 | 50 | 7 | 40 | 40 | 20 |
| T65-50-7 | 65 | 50 | 7 | 32.5 | 32.5 | 35 |
| T50-30-13 | 50 | 30 | 13 | 15 | 35 | 50 |
| T50-70-13 | 50 | 70 | 13 | 35 | 15 | 50 |
| T80-30-13 | 80 | 30 | 13 | 24 | 56 | 20 |
| T80-70-13 | 80 | 70 | 13 | 56 | 24 | 20 |
| T65-50-13 | 65 | 50 | 13 | 32.5 | 32.5 | 35 |
| PC-1 | – | – | 1 | 0 | 0 | 100 |
| PC-7 | – | – | 7 | 0 | 0 | 100 |
| PC-13 | – | – | 13 | 0 | 0 | 100 |

*T* Ternary binder-stabilized mixtures, *PC* Portland cement-stabilized mixtures, ($x$) %Substitution, ($y$) %CL in alternative fraction, ($z$) Curing time-days

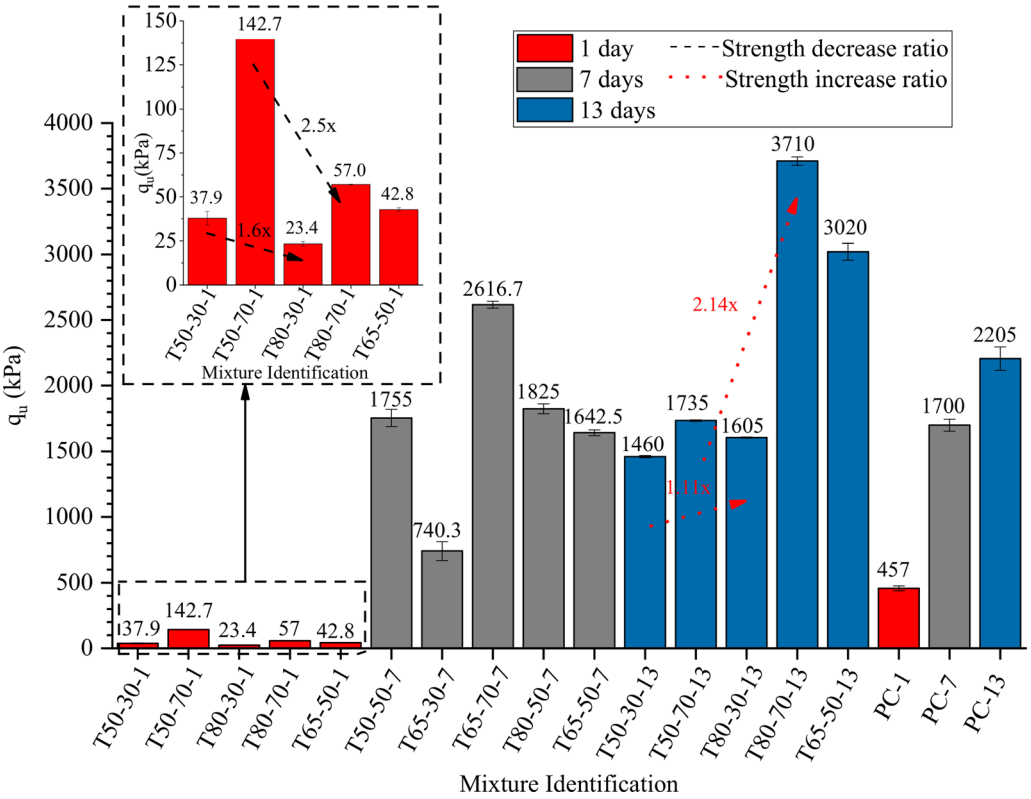


**Fig. 5** Unconfined compressive strength ($q_u$) for each treatment after curing

CEM-III was replaced with GGBS + CL (alternative fraction) by 50–80% by mass (*%Substitution*). The CL content (%CL), varied between 30 and 70% within the alternative fraction. Thermal curing times of 1, 7 and 13 days were adopted. Binder content, soil moisture and the magnitude of preloading in the stabilized soil were defined as constant factors (Table 3), based on the native soil properties and the recommendations proposed by EuroSoilStab [54]. Finally, soil samples stabilized exclusively with CEM-III (in triplicate) were manufactured as reference mixtures, cured under the same study conditions.

## 2.3 Specimens preparation and testing

Fifteen binder designs and three reference mixtures (Table 4) were used to stabilize the organic clay, following the laboratory-scale mass stabilization methodology recommended to simulate in situ conditions [5, 20, 54, 83].

First, the soil was dried and the clods were manually broken into a uniform dry powder. Then, with the help of an electromechanical mixer, the soil was mixed with water to reach the design moisture for 2 min until visual homogeneity was obtained. The binder powder was added and continued to be mixed (for 2 more minutes) with the wet soil until a homogeneous mixture was achieved. The final mixture was placed in a cylindrical mould (20 cm high and internal diameter of 4.75 cm) in 4 layers of approximately 25 mm thickness. Each layer is compacted with light manual pressure three times for approximately 2 s (to eliminate bubbles of liquid or air), until the estimated specimen height of 95 mm was reached. Solid steel bars (with a diameter of 45 mm) were used to apply a preload of 18 kPa after filling the mould, representing 1 m of granular backfill was used as recommended by Axelsson et al. [20] and EuroSoilStab [54].

To simulate the mass stabilization process and curing conditions as accurately as possible, a custom-built sample storage container was manufactured for specimen moulding and curing. The container was automated through the installation of numerous electronic and mechanical components. A programmable thermostat (device '1' in Fig. 4a) was installed to monitor the temperature of water in the container, which controlled the heater (device '2' in Fig. 4a) to ensure that the water temperature was maintained at 59.5–60.5 °C, to accelerate hydration and pozzolanic reactions for strength gain, according to procedures adopted for producing precast GGBS-based concretes [26, 50, 74]. A pair of digital thermometers (device '3' in Fig. 4a) was used to monitor the temperature of the water at different positions within the container. To minimize the

**Table 5** ANOVA table for compressive strength ($q_u$)

| Source | DF | Adj. SS | Adj. MS | *P* value |
|---|---|---|---|---|
| Linear | 3 | 38,415,281 | 12,805,094 | 0 |
| A: % Substitution | 1 | 1,072,651 | 1,072,651 | 0.020 |
| B: % CL | 1 | 5,415,436 | 5,415,436 | 0 |
| C: Curing time | 1 | 31,927,195 | 31,927,195 | 0 |
| Square | 3 | 2,146,132 | 715,377 | 0.015 |
| $A^2$: % Substitution*% Substitution | 1 | 45,044 | 45,044 | 0.618 |
| $B^2$: % CL*% CL | 1 | 396,352 | 396,352 | 0.145 |
| $C^2$: Curing time*Curing time | 1 | 1,778,381 | 1,778,381 | 0.003 |
| Interactions | 3 | 4,021,741 | 1,340,580 | 0.001 |
| AB: % Substitution*% CL | 1 | 411,733 | 411,733 | 0.138 |
| AC: % Substitution*Curing time | 1 | 2,000,633 | 2,000,633 | 0.002 |
| BC: % CL*Curing time | 1 | 1,609,374 | 1,609,374 | 0.005 |
| Error | 33 | 5,874,469 | 178,014 | |
| Lack of fit | 4 | 3,512,312 | 878,078 | 0.110 |
| Pure error | 29 | 2,362,156 | 81,454 | |
| Total | 44 | 54,053,498 | | |
| S (standard deviation) = 421.917 | | | | |
| $R^2$ = 0.891 | | | | |
| $R^2$ (adjusted for free degrees) = 0.855 | | | | |
| $R^2$ (predicted) = 0.809 | | | | |

*DF* Free Degree, *Adj. SS* Adjusted Sum of Squares, *Adj. MS* Adjusted Average of Squares, $R^2$ Coefficient of determination

effects of evaporation on lowering water levels within the storage container, a float valve (device '4' in Fig. 4a) was installed to introduce more water into the container and maintain a constant water level throughout the curing period. To maintain the temperature uniform along all points of the container, a submersible water pump (device '5' in Fig. 4a) was installed to create a water flow to avoid hot water points near the heater. Finally, an overflow pipe (device '6' in Fig. 4a) was installed as a safety measure, to prevent water overflow should the float valve fail.

The base of the container was made of rigid acrylic, so rings (Fig. 4c) were fixed to function as a bottom support for the cylindrical moulds (Fig. 4b), which are equipped with a geotextile at their base to prevent migration of the stabilized soil mixture. These rings allow the cylindrical moulds to be isolated at the base of the container (approximately 1/3 of the height of the ring), below which a series of perforations were made to allow the free circulation of water, through the geotextile, towards the stabilized mixtures during the curing period (curing under immersion). After the specified curing period, with the aid of a specimen extractor, the stabilized mixtures were extruded from the cylindrical moulds.

## 2.4 Unconfined compressive strength tests

Prior to the compression test, the faces of the specimens were cut and/or coated to ensure a flat surface perpendicular to their longitudinal axis and to maintain a height of 9.5 cm [54]. Unconfined compressive strength (UCS) tests were performed according to ASTM D1633-17 [14] in an automatic loading frame (equipped with a 50kN load cell), where a strain rate of 1.14 mm/min was used. The tests were stopped by adopting the maximum compressive stress failure criterion. Mass-stabilized soil specimens were tested after 1, 7 and 13 curing days, as presented in Tables 3 and 4.

## 2.5 Secant modulus of elasticity

Geotechnical designs must be assessed in terms of their ultimate limit state (ULS) and serviceability limit state (SLS) to satisfy international engineering standards (e.g. Eurocode 7). For mass soil stabilization, limit state is governed by deformability conditions, therefore SLS is more relevant than ULS [59, 83]. Hence, Young's (elastic) moduli ($E_{50}$) were measured from compressive stress–axial strain curves generated for all mass-stabilized soil mixtures using the secant method (i.e. for 50% of peak stress of material ($q_u$), in accordance with EuroSoilStab [54].

**Table 6** ANOVA table for stiffness ($E_{50}$)

| Source | DF | Adj. SS | Adj. MS | *P* value |
|---|---|---|---|---|
| Linear | 3 | 666,475 | 297,762 | 0 |
| A: % Substitution | 1 | 14,923 | 14,923 | 0.025 |
| B: % CL | 1 | 98,482 | 98,482 | 0 |
| C: Curing time | 1 | 553,070 | 553,070 | 0 |
| Square | 3 | 16,539 | 5,513 | 0.006 |
| $A^2$: % Substitution*% Substitution | 1 | 566 | 566 | 0.651 |
| $B^2$: % CL*% CL | 1 | 3,280 | 3,280 | 0.279 |
| $C^2$: Curing time*Curing time | 1 | 12,693 | 12,693 | 0.008 |
| Interactions | 3 | 75,728 | 25,243 | 0 |
| AB: % Substitution*% CL | 1 | 11,097 | 11,097 | 0.061 |
| AC: % Substitution*Curing time | 1 | 29,983 | 29,983 | 0.002 |
| BC: % CL*Curing time | 1 | 34,648 | 34,648 | 0.001 |
| Error | 33 | 89,497 | 2,712 | |
| Lack of fit | 4 | 52,803 | 13,201 | 0.090 |
| Pure error | 29 | 36,694 | 1,265 | |
| Total | 44 | 872,239 | | |
| S (standard deviation) = 52.08 | | | | |
| $R^2$ = 0.906 | | | | |
| $R^2$ (adjusted for free degrees) = 0.874 | | | | |
| $R^2$ (predicted) = 0.844 | | | | |

*DF* Free Degree, *Adj. SS* Adjusted Sum of Squares, *Adj. MS* Adjusted Average of Squares, $R^2$ Coefficient of determination

### 2.6 Microstructure and mineralogy

Selected samples of the soil stabilized with the alternative ternary binder (HTB) and CEM-III (HCP) were subjected to mineralogical and microstructural analyses. To avoid the continuation of cementitious reactions of the different binders between the sampling period and the execution of the tests, by means of the solvent substitution technique (using isopropanol) proposed by Scrivener et al. [106], the hydration and pozzolanic reactions (in HCP and HTB samples, respectively) were stopped at a predetermined curing time and object to study, in order to preserve the mineralogy and microstructure for the curing times under study. The mineralogical composition of the specimens was determined by X-ray diffractometry (XRD) by the disoriented powder method [79] using a Bruker D8 ADVANCE X-ray diffractometer in a scanning range of 2°–80° at a step of 0.02°/40 s. In addition, for comparative purposes, mixtures without hydration process (N-HTB and N-HCP) were also analysed in order to identify the formation and evolution of new mineralogical phases. The microstructure of the samples was investigated by scanning electron microscopy (SEM) with energy dispersive X-ray analysis (EDX) using a Jeol JSM-6610LV. Sheet samples were prepared to study the morphology and composition of the reaction products. To maximize the quality of the SEM images, the samples were first dried under vacuum and metallized with gold.

## 3 Results and discussion

### 3.1 Geomechanical strength

Figure 5 summarizes the UCS test results for the different ternary mixtures of the proposed binders [Treatments T(*x*)-(*y*)-(*z*) in Fig. 5] and the results of the mixtures with CEM-III as reference [Treatments PC-(*z*) in Fig. 5]. The findings revealed two important considerations in the geomechanical performance of the mass-stabilized soil mixtures: (1) the importance of thermal curing time in activating pozzolanic reactions; and (2) the relevance of the addition of high calcium contents in the performance of the alternative binder. Regardless of the dosage of the constituents of the TB, it was possible to observe the great evolution of the UCS of the mixtures after 13 days of thermal curing [mixtures T(*x*)-(*y*)-13 in blue colour—Fig. 5], with respect to the mixtures after 7 days and 1 day of thermal curing [mixtures T(*x*)-(*y*)-7 and T(*x*)-(*y*)-1 in grey and red colour, respectively—Fig. 5].

Strength gains of 38–70 times (38× to 70×) were observed with curing time (1–13 days) between treatments or ternary mixtures of equal dosage. Several studies have

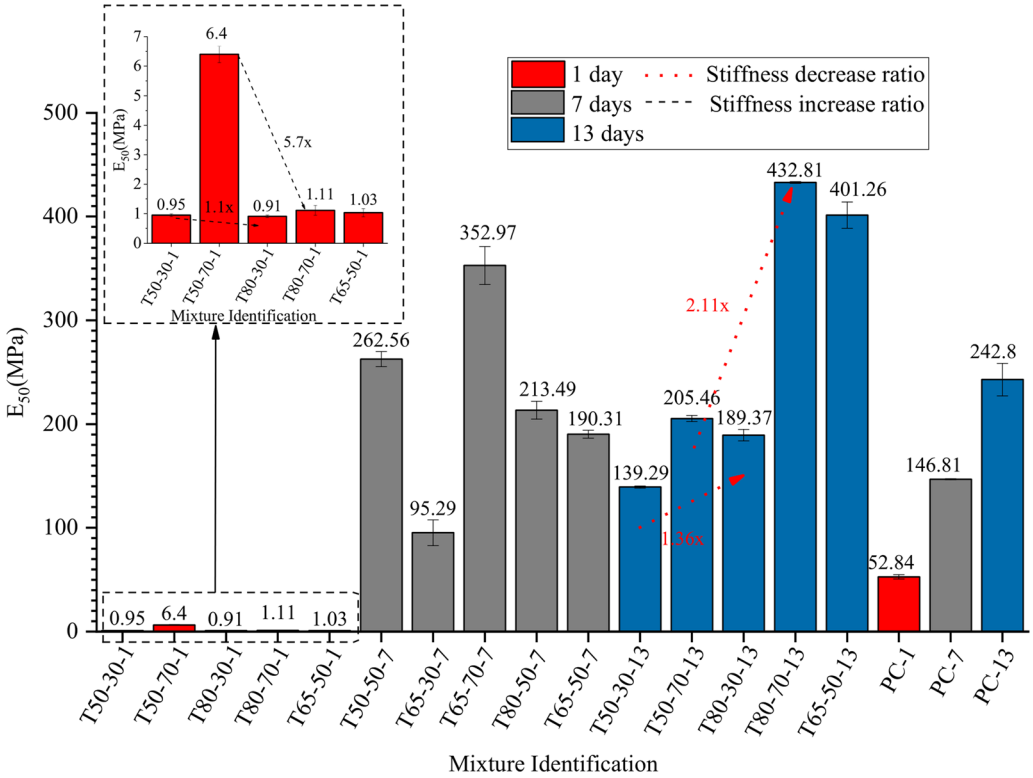


**Fig. 6** Secant elasticity modulus ($E_{50}$) for each treatment after curing

verified that the pozzolanic reaction rate is very low (low initial strengths) [43, 45, 47, 50, 85]. However, the increase in curing temperature enabled a greater amount of aluminosilicates in reactive phases of the slag to react to form cementitious compounds. This was due to the higher solubility of alkaline hydroxides ($Ca(OH)_2$ from the CL) with temperature, which rapidly increased the alkalinity of the system and, consequently, allowed these aluminosilicates in the slag to be released (solubilized), facilitating the formation of cementitious gels [28, 32].

Escalante et al. [52] and Escalante-García and Sharp [53], in Portland cement pastes with GGBS additions (30–50 wt%) observed that the amount of reacted slag increased by up to 20% as the curing temperature increased from 30 to 60 °C after 28 days. This was due to the pozzolanic reaction between GGBS and $Ca(OH)_2$ produced in the same hydration process as Portland cement. The inclusion of temperature in the curing processes (thermal and hydrothermal) in the study of cementitious materials has been catalogued as a catalytic agent of the reactions [41, 122]. In this regard, several authors have studied the implementation of different thermal curing regimes to determine the maximum achievable compressive strength in different types of binders to predict and model their strength development at different ages when cured at ambient conditions [4, 64, 84, 91].

On the other hand, it was observed that the TB mixtures with higher CL contents (%CL $\geq$ 50%) showed the highest strength magnitudes, even when compared with the reference mixtures, mainly after 7 and 13 days of curing (treatments PC-7 and PC-13, respectively—Fig. 5). The maximum failure stress attained in the study (i.e. the maximum unconfined ($UCS_{Max}$) was recorded for the T80-70-13 mixture, reaching 3710 kPa after 13 days of thermal curing. This mixture possessed "% *CL*" = 56 wt%, "*%GGBS* = 24 wt% and "% *CEM-III*" = 20% (Table 4). That is, the mixture with lower CEM-III content and higher %CL in the alternative fraction of study. In addition, it can be observed that T80-70–13 produced a much higher UCS compared to its lower "*%Substitution*" analogous mix (T50-70–13) and the reference mix (PC-13), which used only CEM-III. Similarly, after 7 days of curing, the T65-70–7 mix ("% CL" = 45.5 wt%, "%GGBS = 19.5 wt% and "% CEM-III" = 35%—Table 4) reached a strength of

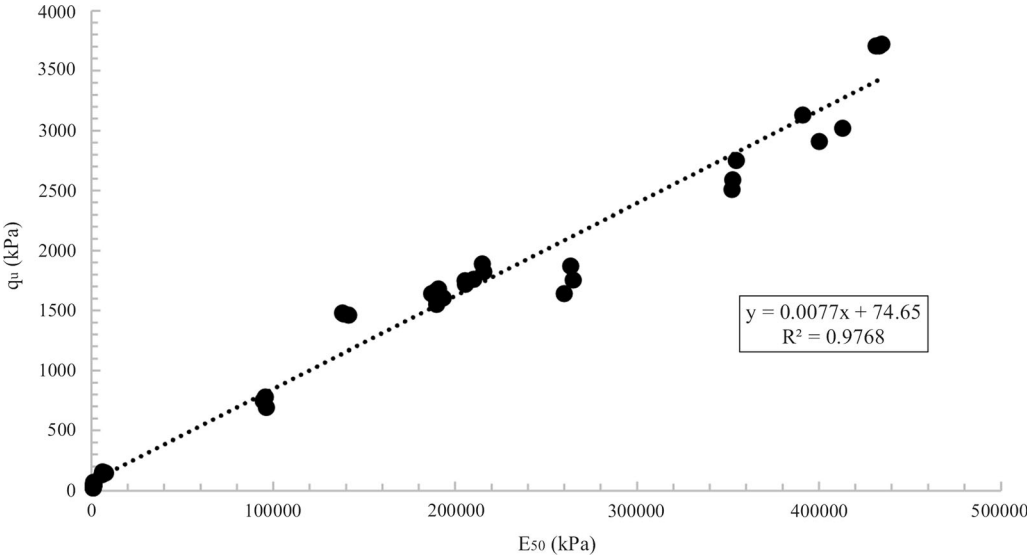


**Fig. 7** Relationship between unconfined compressive strength ($q_u$) and secant elasticity modulus ($E_{50}$)

2616.7 kPa, equivalent to 1.5× the strength of the mix that used exclusively CEM-III (1700 kPa in treatment PC-7). However, after 1 day of curing, the strengths of the reference mix (PC-1 in Fig. 5) tended to be higher compared to the TB mixes [T($x$)-($y$)-1 mixtures in Fig. 5], evidencing the rapid hardening characteristic of Portland clinker-based binders and the need for their inclusion to guarantee a minimum initial strength for practical applications of the mass stabilization method.

Figure 6 presents the corresponding $E_{50}$ measurements. The findings showed a stiffness behaviour similar to that previously reported for strength. The relevance of the curing time and the addition of CL in the mechanical development of the mixtures was highlighted. The maximum stiffness was observed in Mixture T80-70-13, reaching 432.8 MPa, T65-50-13 (401.3 MPa) and T65-70-7 (352,9 MPa). These mixtures had "*% substitution*" of 80% and 65%, "*% CL*" = 70% and 50%, after 13 and 7 days of thermal curing, respectively. Furthermore, these three mixtures produced higher stiffnesses compared with the CEM-III reference mixtures (PC-13 and PC-7, respectively—Fig. 6). The $q_u$ results and $E_{50}$ measurements from this study were directly correlated with each other, as presented in Fig. 7 which presented a linear behaviour defined by a coefficient of determination, $R^2 = 0.97$, with a $E_{50}/q_u$ ratio between 100 and 200 times in agreement EuroSoilStab [54]. This linear correlation between $q_u$ and stiffness was also observed by Lemos et al. [83] when using $E_{50}$, and by Consoli et al. [44] and Lotero et al. [85] who used initial shear modulus ($G_0$) as the stiffness parameter.

## 3.2 Statistical analysis and multivariate regression analysis (MRA)

An analysis of variance (ANOVA) was used to statistically evaluate the significance of the controllable factors (linear and/or quadratic effect) and their interactions on the response variables. The statistical significance (α) adopted for the ANOVA was 0.05 (or 5%), i.e. a 95% confidence level. The ANOVA results for $q_u$ and $E_{50}$ are presented in Tables 5 and 6, respectively. Equations (1) and (2) define the $q_u$ and $E_{50}$, respectively; where $A$ is the "*% Substitution*", $B$ is the "*% CL*" within the alternative fraction and $C$ is the "*Curing time*". These equations, for practical purposes, allowed the prediction of the mechanical response of the ternary binder across different levels of the variables under study and therefore the construction of response surfaces. The regression model defining the response surfaces (Figs. 8 and 9) was validated using the values of the coefficient of determination adjusted to the degrees of freedom of the statistical model ($R^2adj$). The values of $R^2adj = 0.855$ and $R^2adj = 0.874$ obtained from the MRA were notably higher than the $R^2adj = 0.7$ recommended by Montgomery [89] for response variable prediction purposes. Additionally, the non-significance of the ANOVA lack of fit ($P$ value > 0.05 in Tables 5 and 6, respectively) determined that the quadratic model proposed

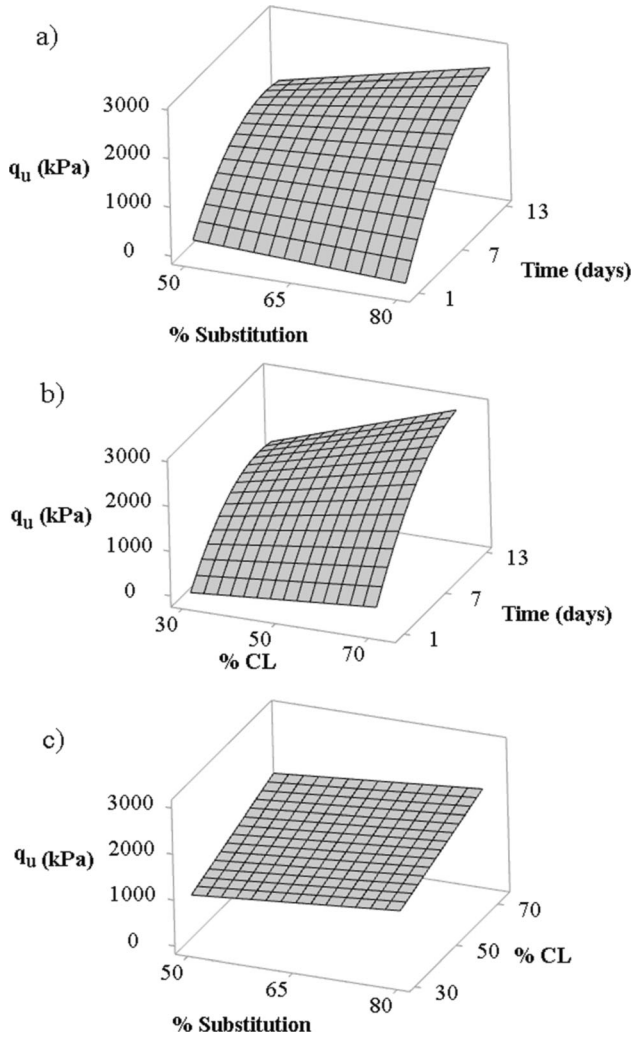


**Fig. 8** Unconfined compressive strength response surfaces for **a** Curing time (days) versus % Substitution; **b** %CL versus Curing time (days); and **c** %CL versus % Substitution

in the experimental design (CCD) adequately fits the experimental data.

$$q_u(\text{kPa}) = 53 - 9.85A + 6.14B + 66C - 15.07C^2 + 3.21AC + 2.16BC \quad (1)$$

$$E_{50}(\text{MPa}) = 21 - 1.26A + 0.648B - C - 1.27C^2 + 0.393AC + 0.3166BC \quad (2)$$

The ANOVA ratified, both for $q_u$ and $E_{50}$, the great influence of curing time on the mechanical response of the stabilized soil, through the high values in the adjusted mean squares (Adj. MS) of the different effects related to this factor (factor C in Tables 5 and 6, respectively). The response surfaces in Figs. 8a, b and 9a, b illustrated the initial linear increase (first 7 days of curing) of the mechanical response (for $q_u$ and $E_{50}$, respectively) and subsequently an asymptotic trend for the 13 days of thermal curing, independently of the *%Substitution* and *%CL* of the binder. This behaviour was validated by the statistical significance ($P$ value $< 0.05$) of both the linear ($C$) and quadratic ($C^2$) effect of the variable, showing a strong indication that future strengths were achieved within 13 days of thermal curing. These results were of great relevance, as the slow reaction rate of pozzolanic binders can continue for many months or years under room temperature curing conditions [104]. This hinders preliminary investigations (design and dosing of the cementitious agent) at laboratory scale to make practical applications of the mass stabilization technique feasible [54, 59, 78].

The significant interaction effect of the factors "*% substitution*" and "*Curing time*" for $q_u$ and $E_{50}$ (*AC* interaction in Tables 5 and 6, respectively) confirmed that CEM-III improved the initial mechanical behaviour and, the pozzolanic part, the long-term strength and stiffness development. The response surfaces (Figs. 8a and 9a) showed that after 1 day of curing, binder mixes containing 50% CEM-III resulted in average strength and stiffness values between 1.6 and 5.3 times higher than for mixes with 20% CEM-III, regardless of the %CL (T50-30–1/T80-30-1 and T50-70-1/T80-70-1 ratios in Figs. 5 and 6), while for 13 days of curing, the mixes with 20% CEM-III resulted in $q_u$ and $E_{50}$ values between 1.1 to 2.1 times higher than for the mixes with 50% CEM-III (T80-30–13/T50-30-13 and T80-70-13/T50-70-13 ratios in Figs. 5 and 6). This indicated that the addition of the alternative binder fraction has a positive influence on long-term strength performance, thus facilitating the reduction of the CEM-III content in cementitious agent designs. However, its total elimination is inadvisable for engineering scenarios where short-term strength gains are a priority.

On the other hand, the results showed that the factor "*%CL*" generated a linear growth in the mechanical response, i.e. increasing the CL content linearly increases the magnitude of $q_u$ and $E_{50}$, regardless of the percentage of CEM-III substituted by the alternative fraction (Figs. 8c and 9c, respectively). This could be verified by the exclusive statistical significance ($P$ value $> 0.05$) of their linear effect ($B$), in Tables 5 and 6, respectively. However, the need for a high calcium content within the TB was observed to activate GGBS and maximize qu and E50 with curing time (BC interaction effect in Tables 5 and 6), as illustrated in Fig. 8b and 9b, respectively. This behaviour could be explained by the acidic pH, organic content (approximately 10%) and the type of soil (clay) to be stabilized, which would collectively reduce the reactivity of the binder when mixed with the soil [21, 22, 29, 77].

Similarly, the moulding and curing methodology adopted, in which the soil is saturated, and water is available during the curing process (simulating the in situ conditions of mass stabilization), would also justify the high CL

requirements. A higher water content in the reaction decreases the strength of the pozzolanic binder [60]. In addition, a pH value > 10.5 in the soil–cement mixture is required for the pozzolanic reaction to occur [51, 92].

### 3.3 Microstructure and mineralogy

The stabilized clay mixtures that produced the best mechanical behaviour using ternary binder (HTB) and CEM-III (HPC) were selected for microstructural and mineralogical investigation of reaction products (treatments or mixtures T80-70-13 and PC-13, respectively). Likewise, non-hydrated samples of the same treatments of both ternary binder (N-HTB) and CEM-III (N-HCP) were selected, as was argued, with the objective of identifying the formation and evolution of the reaction products at a mature age (after thermal curing) and to investigate the morphology and microstructure of the stabilized mixtures.

#### 3.3.1 XRD analyses

The mineralogical phases present in the stabilized mixtures were identified through detailed inspection of the peaks within their respective XRD spectra via the Inorganic Crystal Structure Database [71], which were also compared to the spectra produced for the raw soil, the starting materials (Fig. 2) and the non-hydrated mixtures (Fig. 10). For the N-HTB sample, portlandite and calcite (mainly from CL), quartz and phyllosilicates (from soil) and alite/belite (from CEM-III) were the predominant mineral phases observed. After the hydration and thermal curing process (HTB mixtures), the XRD spectra suggested that the original portlandite and alite/belite reacted to form new reaction products, characterized by having cementitious properties and a semi-crystalline structure and/or low degree of ordering (broader—"flared" and low intensity peaks) such as hydrated calcium silicate/aluminate (C–S–H/C–(A)–S–H), hydrotalcite, metastable amorphous calcium carbonate and hydrated calcium hemicarboaluminate (Fig. 10a), evidencing the thermodynamic instability typical of compounds in formation. The portlandite was completely consumed, indicating a high level of pozzolanic reaction between the components of the CL and the GGBS, thus explaining the higher strengths obtained by this binder after thermal curing.

These reaction products were compounds resulting from both the hydration process of CEM-III and the alkaline activation of GGBS (pozzolanic reaction). Taylor [114] related the majority presence of C–S–H/C–(A)–S–H) and minority presence of metastable amorphous calcium carbonate and hydrotalcite in the reaction products of Portland cement. On the other hand, Seo et al. [108] observed the presence of hemicarbonate, hydrotalcite and C–(A)–S–H

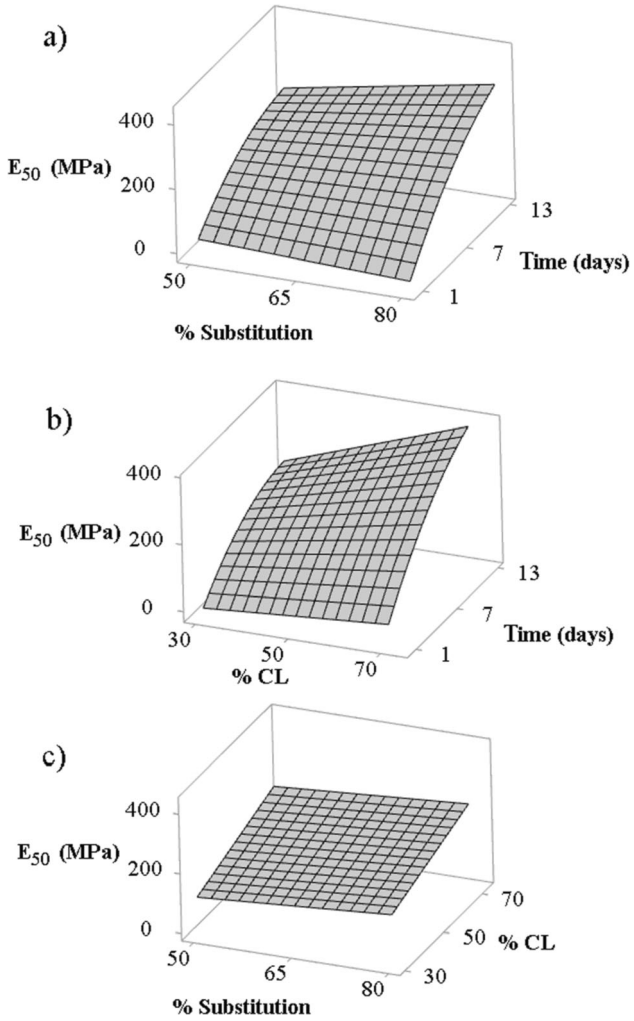


**Fig. 9** Secant elasticity modulus response surfaces for **a** Curing time (days) versus % Substitution; **b** %CL versus Curing time (days); and **c** %CL vs %Substitution

phases in slag and carbide residue mixtures. The coexistence of these various reaction products in the same cementitious matrix, synthesized through different chemical reaction mechanisms (hydration and alkaline activation), has been commonly referred to in the literature as blended cements [111, 112].

On the other hand, for the N-HCP, the key mineral phases observed were alite ($C_3S$), belite ($C_2S$), portlandite ($Ca(OH)_2$), tetracalcium ferroaluminates ($C_4AF$) and tricalcium aluminates ($C_3A$) from CEM-III, as well as quartz and some phyllosilicates (m, M, Fh, K in Fig. 10b) from the soil. After the hydration and thermal curing process, XRD spectra of the HCP sample determined that CEM-III reacted forming mainly C–S–H/C–(A)–S–H and ettringite phases, as similarly observed in Taylor [114] and Jennings [73], with other minority carbonate phases of calcite and hydrated calcium hemicarboaluminate. However, in the

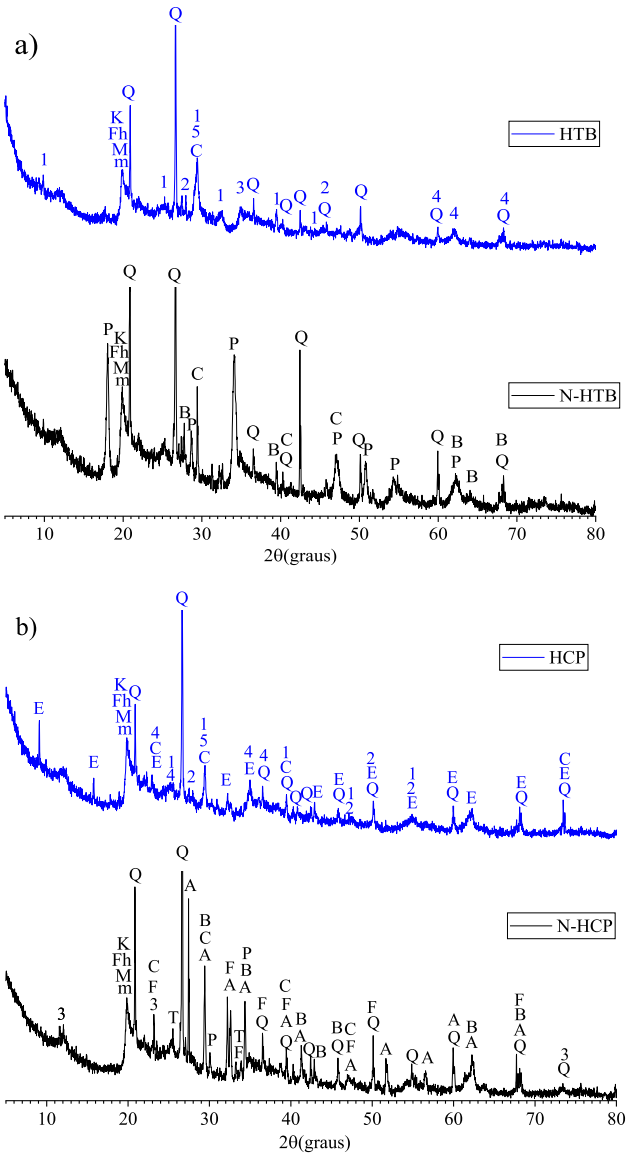


**Fig. 10** XRD spectra of **a** ternary binder hydrated (HTB) and non-hydrated (N-HTB) and, **b** Portland cement hydrated (HCP) and non-hydrated (N-HCP) after 13 days of thermal curing. A: Alite-C3S (tricalcium silicate); B: belite-C2S (dicalcium silicate); C: calcite; E: ettringite; F: C4AF (tetracalcium aluminoferrite); Fh: ferrihydrite; K: kaolinite; m: muscovite; M: Montmorillonite; P: portlandite; Q: quartz; T: C3A (tricalcium aluminate); 1: CASH (calcium aluminate silicate hydrate); 2: CSH (calcium silicate hydrate); 3: hydrotalcite; 4: calcium hemicarboaluminate hydrate; 5: metastable amorphous calcium carbonate

HTB mixtures a better definition and greater intensity of the peaks or diffraction lines of the compounds was observed. This was indicative of a greater quantity and degree of polymerization of the gels formed in the stabilized soil, which would be associated with the high magnitudes of $q_u$ and $E_{50}$ previously reported for the ternary mixtures.

### 3.3.2 SEM

Figure 11 presents the SEM micrographs (morphology) of the HTB (Fig. 11a–c) and HPC (Fig. 11d–f) mixtures at magnifications of ×500, ×1000 and ×2000, corresponding to the T80-70-13 and PC-13 treatments of the experimental program, respectively. In general, the micrographs indicated that the stabilized soil mixtures generated homogeneous matrices due to the cementation levels after thermal curing. However, the samples stabilized with the ternary binder (HTB) showed a lower amount of micropores and macropores. This explains the excellent mechanical performance of the soil stabilized with the ternary binder compared to the CEM-III mixtures by accelerating the reactions with thermal curing. Porosity strongly influenced strength development and is considered as a key factor in the mechanical behaviour of artificially cemented soils [33–39, 42–46]. These findings would be linked to the further evolution of cementitious reaction products resulting from the hydration process of the CEM-III fraction and alkaline in activation of GGBS HTB mixtures, previously reported from XRD analyses.

The SEM micrographs presented in Fig. 12a (×3500) identified typical C–S–H/C–(A)–S–H) gel morphologies, formed by the hydration of CEM-III (HPC) at a mature age (due to thermal curing). These corresponded to structures in the form of solidified sheets (Pt. A), interwoven "honeycomb" sheets (Pt. B) and amorphous agglomerates (Pt. C), evidencing the geliform characteristic (variable morphology) of this reaction product [81, 97, 98]. EDX spectra (e.g. E-1 and E-2 in Fig. 12b and c), respectively), taken pointwise, showed a slight inclusion of aluminium (*Al*) within the C-S–H gel (C–(A)–S–H gel) which guarantees the rapid initial setting of CEM-III. In addition, high calcium (*Ca*) contents, with atomic *Ca/Al* ratios ≥ 1.0, define the characteristic low degree of polymerization of these gels (lamellar structures—formed by $Q^2$ units) [61, 106]. On the contrary, Fig. 13a shows the formation of a C-A-S–H gel of dense and homogeneous structure (lower porosity), rich in aluminium, with *Ca/Al* ratios < 1.0 (spectra E-3 and E4 in Fig. 13b and c, respectively) showing the advanced degree of the pozzolanic reaction and structural order in which the aluminosilicates are arranged within the gel after thermal curing. This evidenced the effectiveness of the curing methodology to accelerate the reactions of the HTB mixtures and to determine their mechanical behaviour after long curing periods.

## 3.4 Thermal curing analysis

Using thermal curing, the use of a TB composed of 20% CEM-III, 56% CL and 24% GGBS (T80-70-13 treatment in Table 4) led to the highest mechanical response in the

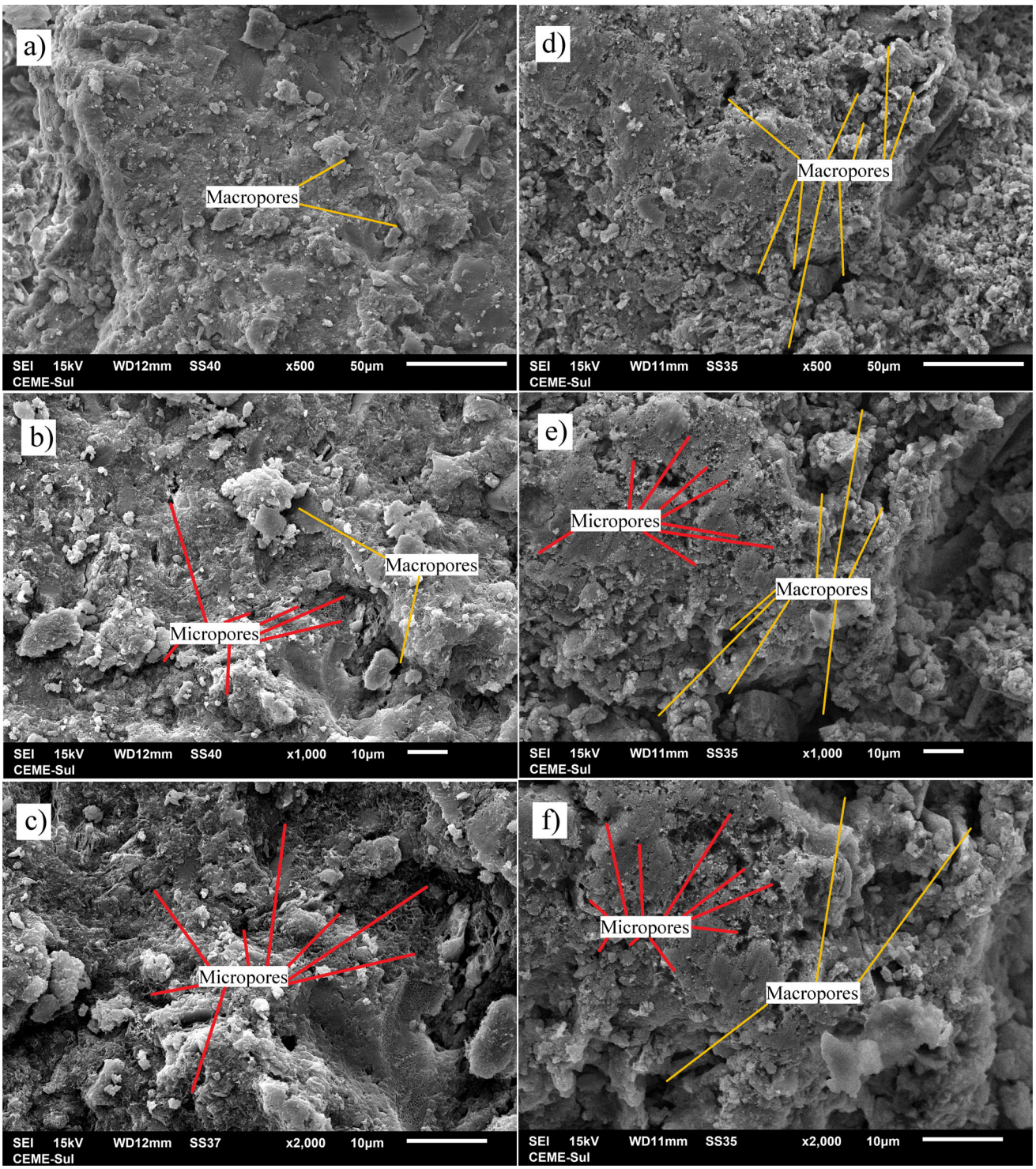


**Fig. 11** SEM micrographs of soil stabilized with **a** HTB – × 500, **b** HTB –×1000, **c** HTB – ×2000, **d** HCP – ×500, **e** HCP – ×1000, **f** HCP – ×2000

study. Curing temperature (60 °C) played a key role along with curing time in the production of cementitious reaction products and in increasing strength and stiffness. Therefore, to experimentally validate the findings from statistical analysis and to determine the role of thermal curing versus a potential curing at room temperature

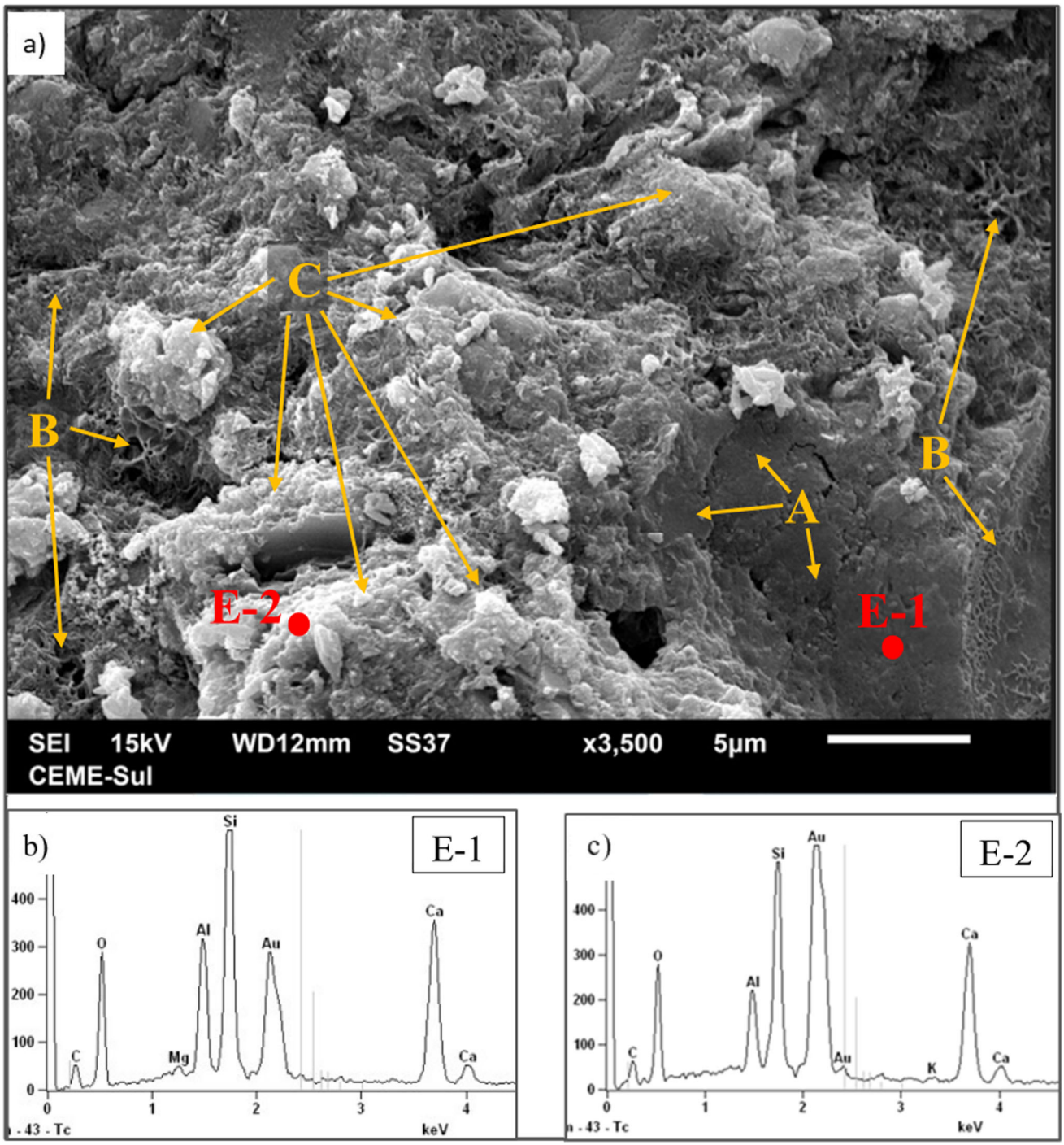


**Fig. 12** SEM micrographs of soil stabilized with CEM-III at: **a** magnification ×3500; **b** EDX spectra of point E-1 and **c** EDX spectra of point E-2

(in situ conditions), an evaluation of the development of $q_u$ after the specimens were cured at a controlled temperature of 20 °C (HTB-20 °C in Fig. 14) was proposed for this ternary mix (T80-70–13). The previously implemented laboratory-scale moulding and curing methodology (under immersion) was used. This was done to simulate ambient curing conditions after 1, 7, 28, 60 and 90 days. Similarly, thermally cured specimens (HTB-60 °C in Fig. 14) were tested at 1, 7, 13, 28 and 60 days of curing. In parallel, these tests were replicated for the 100% CEM-III stabilized soil mix (treatment PC-13), in order to verify and contrast the development of its strength under the two curing

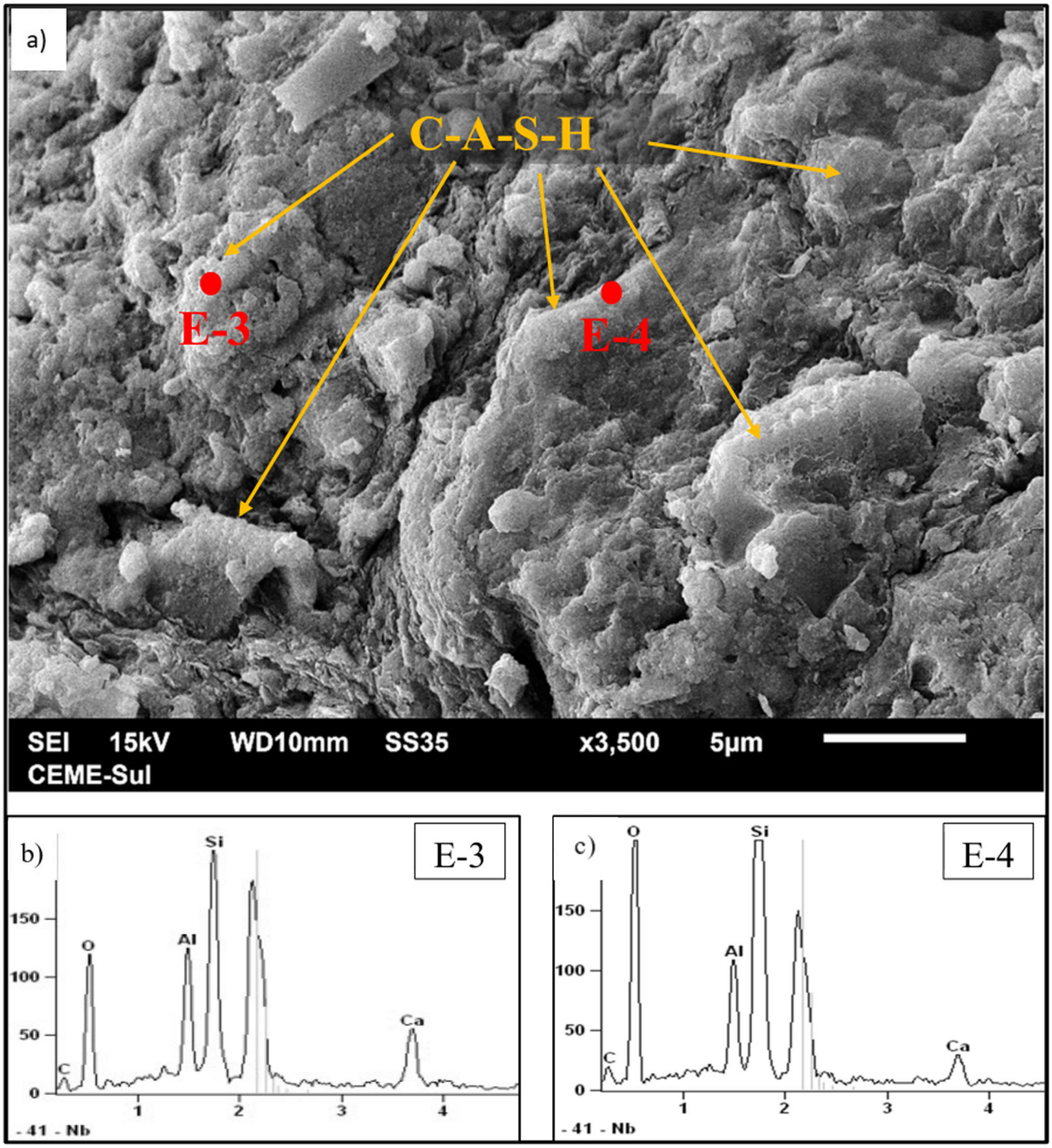


**Fig. 13** SEM micrographs of soil stabilized with TB at: **a** magnification ×3500; **b** EDX spectra of point E-3 and **c** EDX spectra of point E-4

conditions (thermal: HPC-60 °C and room temperature: HPC-20 °C in Fig. 14).

Figure 14 shows the results of curing time versus $q_u$ (average of three replicates), showing the importance of the type of binder. The HTB mixtures produced higher long-term strengths than CEM-III (HPC), as observed in the statistical analysis, regardless of the curing regime. The $q_u$ obtained for the HTB-20 °C mixtures after 90 days of curing still did not reach the $q_u$ recorded for the equivalent samples that had been thermally cured for 13 days (HTB-60 °C). Furthermore, it was observed that the HTB-60 °C mixtures practically developed their maximum strength at

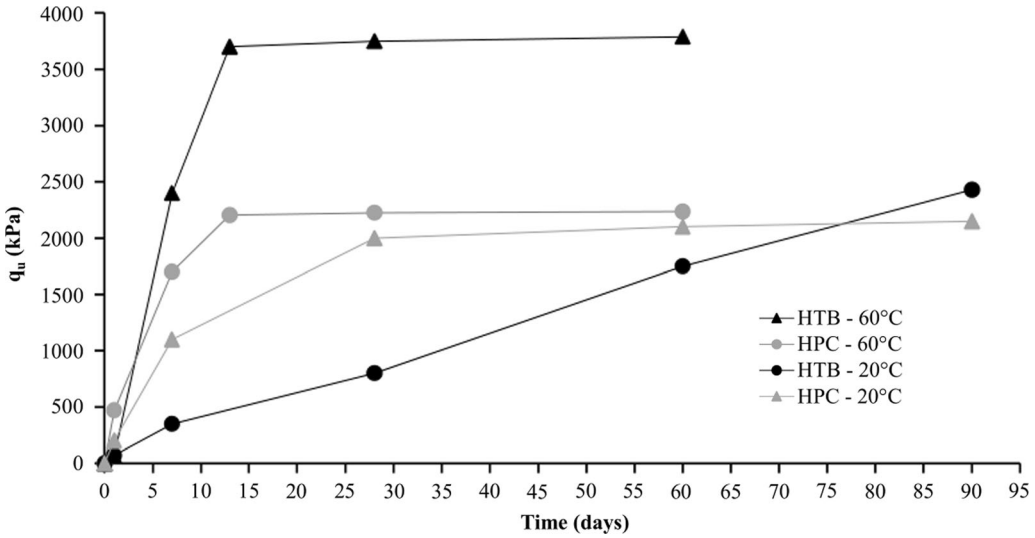


**Fig. 14** Curing time versus $q_u$ for thermal and room temperature curing using HTB and HPC

13 days of curing. This served as confirmation that thermal curing successfully simulated the long-term strength (more than 90 days) of the stabilized mass of a clayey organic soil using a TB, verifying its pozzolanic behaviour, with slowly increasing strengths when cured at room temperature (HTB-20 °C).

The stabilized soil mixes using 100% CEM-III did not show this behaviour, reaching the maximum strength after approximately 28 days for a 20 °C cure (HPC-20 °C), when compared to the thermally cured mixes (HPC-60 °C). However, at 7 days of curing the HPC-20 °C mixes reached about 60% of their maximum strength (high early strength). For geotechnical purposes, the use of the TB as an additive in the mass stabilization method was successful, reaching in about 75 days the same $q_u$ as soil stabilized with the commercial binder (CEM-III) in 28 days, when cured at room temperature (20 °C). Similar (or even longer) time periods are required by other techniques for the stabilization of soft soils, such as preloading embankments or vertical drains, to increase the effective stresses and thus the strength of the soil through the consolidation process [8]. This makes the practical application of the mass soil stabilization method feasible through the use of the TB under study.

## 4 Conclusions

From the investigations mentioned in this study, the following conclusions can be drawn:

- $q_u$ and $E_{50}$ of stabilized organic clay specimens were strongly dependent of curing time, confirming the hypothesis that the new ternary binder proposed requires almost 2 weeks for reactions to initiate and strength development to be observed due to its high pozzolana content. CEM-III composing TB successfully ensured short-term strength gains, thereby allowing TB practical use for geotechnical field applications. Mechanical response results for TB were considered satisfactory in relation to reference specimens executed in same conditions, however using a conventional binder (Portland cement) to stabilize an organic clayey soil.
- CL content in TB had a notable influence on stabilized specimens, producing higher values of $q_u$ and $E_{50}$ the higher its content, mainly when thermally cured for longer time periods. The portlandite content of CL was likely responsible for this behaviour, given that it dissolves in aqueous medium and released ions ($OH^-$) to increase the pH and forming reaction products (i.e. alkali activation of GGBS). Longer CL dissolution times result in more stronger reaction products, which increases further with time (pozzolanic reactions).
- Mineralogical and microstructural analyses suggested that ternary binder materials fully reacted to form gels C–A–S–H, along with other new mineral phases including hydrotalcite, metastable amorphous calcium carbonate and hydrated calcium hemicarboaluminate, which likely explain the impressive geomechanical behaviour of TB. This was also confirmed by SEM imaging, which confirmed that stabilization produced a denser and less porous microstructure in TB specimens compared with the CEM-III stabilized soil.
- Using a thermal curing (60 °C) was an important innovative method in mass stabilization to analyse

longer term future strength development in the confines of time-restricted laboratory investigation. This allows geotechnical practitioners to better study and define the binder design and dosage before on-site execution, given that pozzolanic binders have slow rates of reactions. The strength development observed for the mass-stabilized organic clay could be described by an asymptotic trend over the 13 days of thermal curing. This successfully demonstrated the use of short-term thermal curing to simulate the strength development of TB-stabilized soil mixtures cured at room temperature for periods exceeding 90 days.

- Further studies can be carried out in the future to verify the influence of preload level and amount of binder in the mechanical response of stabilized soil. Furthermore, the environmental impact of the proposed ternary binder can be evaluated by life cycle assessment (LCA). Moreover, future studies could check if the current results can be applied to different alternative binders composed by others industrial wastes (e.g. sugarcane bagasse ash, fly ash, rice husk ash, eggshell lime and so on).

**Acknowledgements** The authors wish to explicit their appreciation to MCT-CNPq (Editais INCT-REAGEO & Produtividade em Pesquisa) and MEC-CAPES (PROEX) for the support to the research group.

## Declarations

**Conflict of interest** The authors declare that they have no conflict of interest.

## References

1. Abdila SR, Abdullah MMAB, Ahmad R, Burduhos Nergis DD, Rahim SZA, Omar MF, Sandu AV, Vizureanu P (2022) Potential of soil stabilization using ground granulated blast furnace slag (GGBFS) and fly ash via geopolymerization method: a review. Materials 15:375. https://doi.org/10.3390/ma15010375
2. Adesina A (2020) Recent advances in the concrete industry to reduce its carbon dioxide emissions. Environ Chall 1:100004. https://doi.org/10.1016/j.envc.2020.100004
3. Ahmad A, Sutanto MH, Ahmad NR, Bujang M, Mohamad ME (2021) The implementation of industrial byproduct in Malaysian peat improvement: a sustainable soil stabilization approach. Materials 14:7315. https://doi.org/10.3390/ma14237315
4. Ahmed HU, Mohammed AS, Mohammed AA, Faraj RH (2021) Systematic multiscale models to predict the compressive strength of fly ash-based geopolymer concrete at various mixture proportions and curing regimes. PLoS ONE 16(6):e0253006. https://doi.org/10.1371/journal.pone.0253006
5. Ahnberg H, Bengstsson PE, Holm G (2001) Effect of initial loading on the strength of stabilised peat. Ground Improv 5:35–40
6. Ahnberg H, Johansson S, Pihl H, Carlsson T (2003) Stabilising effects of different binders in some Swedish soil. Ground Improv 7:9–27
7. Alexandre E, Luz CA (2020) Substituição parcial do cimento CPV-ARI por lodo de estação de tratamento de água (ETA) (in portuguese). Matéria 25 (1)
8. Almeida MSS, Marques MES (2013) Design and performance of embankments on very soft soils. CRC Press Taylor & Francis Group
9. ASTM (2014) Standard Test Methods for Specific Gravity of Soil Solids by Water Pycnometer. ASTM D854-14 West Conshohocken Philadelphia
10. ASTM (2015) Standard Practice for Classification of Soils and Soil-Aggregate Mixtures for Highway Construction Purposes. ASTM D3282-15 West Conshohocken Philadelphia
11. ASTM (2017a) Standard practice for classification of soils for engineering purposes (Unified Soil Classification System). ASTM D2487-17e1 West Conshohocken Philadelphia
12. ASTM (2017b) Standard Test Method for Particle-Size Distribution (Gradation) of Fine-Grained Soils Using the Sedimentation (Hydrometer) Analysis. ASTM D7928-17 West Conshohocken Philadelphia
13. ASTM (2017c) Standard Test Method for Particle-Size Distribution (Gradation) of Soils Using Sieve Analysis. ASTM D6913-17 West Conshohocken Philadelphia
14. ASTM (2017d) Standard Test Methods for Compressive Strength of Molded Soil-Cement Cylinders. ASTM D1633-17 West Conshohocken Philadelphia
15. ASTM (2018) Standard Test Methods for Liquid Limit, Plastic Limit, and Plasticity Index of Soils. ASTM D4318-17e1 West Conshohocken Philadelphia
16. ASTM (2019a) Standard Test Methods for pH of Soils. ASTM D4972-19 West Conshohocken Philadelphia
17. ASTM (2019b) Standard specification for Portland cement. ASTM C150 West Conshohocken Philadelphia
18. ASTM (2019c) Standard Test Methods for Laboratory Determination of Water (Moisture) Content of Soil and Rock by Mass. ASTM D2216-19 West Conshohocken Philadelphia
19. ASTM (2020) Standard Test Methods for Determining the Water (Moisture) Content, Ash Content, and Organic Material of Peat and Other Organic Soils. ASTM D2974-20e1 West Conshohocken Philadelphia
20. Axelsson K, Johansson S, Andersson R (2002) Stabilization of organic soils by cement and pozzolanic reactions–Feasibility study. Report 3 Swedish Deep Stabilization Research Centre
21. Bate B, Zhao Q, Burns S (2014) Impact of organic coatings on the frictional strength of organically modified clay. J Geotech Geoenviron Eng 140(1):228–236
22. Bergado DT, Anderson LR, Miura N, Balasubramanian AS (1996) Soft ground improvement in lowland and other environments. American Society of Civil Engineers–ASCE Press Reston VA
23. Bernal SA, Provis JL, Walkley B, San Nicolas R, Gehman JD, Brice DG, Kilcullen AR, Duxson P, van Deventer JSJ (2013) Gel nanostructure in alkali-activated binders based on slag and fly ash, and effects of accelerated carbonation. Cem Concr Res 53:127–144
24. BS (2006) Ground granulated blast furnace slag for use in concrete, mortar and grout–Part 1: Definitions, specifications and conformity criteria. British Standard BS EN 15167-1:2006 United Kingdom
25. Bruschi GS, Santos CP, Ferrazzo ST, Araújo MT, Consoli NC (2021) Parameters controlling loss of mass and stiffness degradation of green stabilized bauxite tailings. In: Proceedings of the institution of civil engineers-geotechnical engineering, pp 1–21. https://doi.org/10.1680/jgeen.21.00119

26. Camarini G (1995) Desempenho de misturas cimento Portland e escória de alto-forno submetidas a cura térmica (in portuguese). Tese (doutorado)–USP–Programa de Pós-Graduação em Engenharia Civil
27. Cardoso FA, Fernandes HC, Pileggi RG, Cincotto MA, Vanderley MJ (2009) Carbide lime and industrial hydrated lime characterization. Powder Technol 195:143–149
28. Castellano CC, Bonavetti VL, Irassar EF (2010) Influence of curing temperature: hydration and strength of cement paste with granulated blast furnace. Matéria 15(4):516–526. https://doi.org/10.1590/S1517-70762010000400004
29. Chen H, Wang Q (2006) The behavior of organic matter in the process of soft soil stabilization using cement. Eng Geo Environ 65(4):445–448
30. Cirino MAG (2016) Estudo de pastas de cimento Portland com adições de cinzas de carvão mineral para uso na cimentação de poços de petróleo (in Portuguese). Dissertação (Mestrado) Universidade Federal do Ceará
31. Coelho MAM, Silva MG, Souza FLS, Sarmento R, Zandonade E, Marimoto T, Helmer JL (2006) Estudo das propriedades e avaliação ambiental de estrutura hidráulica confeccionada com escória de alto-forno ativada quimicamente (in portuguese). SEMENGO
32. Corrêa-Silva M, Miranda T, Rouainia M, Araújo N, Glendinning S, Cristelo N (2020) Geomechanical behaviour of a soft soil stabilised with alkali-activated blast-furnace slags. J Clean Prod 267:122017. https://doi.org/10.1016/j.jclepro.2020.122017
33. Consoli NC, Foppa D, Festugato L, Heineck KS (2007) Key parameters for strength control of artificially cemented soils. J Geotech Geoenviron Eng 133(2):197–205. https://doi.org/10.1061/(ASCE)1090-0241(2007)
34. Consoli NC, Lopes LS Jr, Heineck KS (2009) Key parameters for the strength control of lime stabilized soils. J Mater Civ Eng. https://doi.org/10.1061/(ASCE)0899-1561(2009)21:5(210)
35. Consoli NC, Cruz RC, Floss MF, Festugato L (2010) Parameters controlling tensile and compressive strength of artificially cemented sand. J Geotech Geoenviron Eng 136(5):759–763. https://doi.org/10.1061/(ASCE)GT.1943-5606.0000278
36. Consoli NC, Rosa AD (2010b) Parameters controlling strength of coal fly ash-lime improved soil. In: GeoFlorida 2010: advances in analysis modelling e design, pp 89–98
37. Consoli NC, Rosa AD, Corte MB, Lopes LS Jr, Consoli BS (2011) Porosity cement ratio controlling strength of artificially cemented clays. J Mater Civ Eng 23(8):1249–1254. https://doi.org/10.1061/(ASCE)MT.1943-5533.0000283
38. Consoli NC, Rosa AD, Saldanha RB (2011) Parameters controlling strength of industrial waste-lime amended soil. Soils Found 51(2):265–273
39. Consoli NC (2014) A method proposed for the assessment of failure envelopes of cemented sandy soils. Eng Geol 169:61–68
40. Consoli NC, Rocha CG, Saldanha RB (2014) Coal fly ash – carbide lime bricks: An environment friendly building product. Constr Build Mater 69(2014b):301–309
41. Consoli NC, da Rocha CG, Silvani C (2014) Effect of curing temperature on the strength of sand, coal fly ash, and lime blends. J Mater Civ Eng 26(8):06014015
42. Consoli NC, Ferreira PM, Tang C, Marques SFV, Festugato L, Corte MB (2016) A unique relationship determining strength of silty/clayey soils: Portland cement mixes. Soils Found 56(6):1082–1088
43. Consoli NC, Paula TM, Bortolotto MS, Barros LM, Pereira F, Rocha MM (2017) Coal fly ash–carbide lime admixtures as an alternative to concrete masonry blocks: Influence of ash ground. J Mater Civ Eng 29(2):04016224
44. Consoli NC, Winter D, Leon HB, Scheuermann Filho HC (2018) Durability, strength, and stiffness of green stabilized sand. J Geotech Geoenviron Eng 144(9):04018057. https://doi.org/10.1061/(asce)gt.1943-5606.0001928
45. Consoli NC, Carretta MS, Leon HB, Scheuermann Filho HC, Tomasi LF (2019) Strength and stiffness of ground waste glass-carbide lime blends. J Mater Civ Eng 31(10):06019010
46. Consoli NC, Saldanha RB, Scheuermann Filho HC (2019) Short- and long-term effects of sodium chloride on strength and durability of coal fly ash stabilized with carbide lime. Can Geotech J 56(12):1929–1939. https://doi.org/10.1139/cgj-2018-0696
47. Consoli NC, Daassi-Gli CAP, Ruver CA, Lotero A, Scheuermann Filho HC, Moncaleano CJ, Lourenço DE (2021) Lime-ground glass-sodium hydroxide as an enhanced sustainable binder stabilizing silica sand. J Geotech Geoenviron Eng 147(10):06021011
48. Consoli NC, Vogt JC, Silva JPS, Chaves HM, Scheuermann Filho HC, Moreira EB, Lotero A (2022) Behaviour of compacted filtered iron ore tailings-portland cement blends: New Brazilian trend for tailings disposal by stacking. Appl Sci 12:836. https://doi.org/10.3390/app12020836
49. Consoli NC, Silvano LW, Lotero A, Scheuermann Filho HC, Moncaleano CJ, Cristelo N (2022) Key parameters establishing alkali activation effects on stabilized rammed earth. Constr Build Mater 345:128299. https://doi.org/10.1016/j.conbuildmat.2022.128299
50. Cyr M, Patapy C (2016) Synergic effects of activation routes of ground granulated blast-furnace slag (GGBS) used in the precast industry. HAL Open Science
51. Davidson LK, Demirel T, Handy RI (1965) Soil pulverization and lime migration in soil lime stabilization. Highway Res Rec 92:103–126
52. Escalante JI, Gómez L, Ojal KK, Mendoza G, Mancha H, Méndez J (2001) Reactivity of blast-furnace slag in portland cement blends hydrated under different conditions. Cem Concr Res 31(10):1403–1409
53. Escalante-García JI, Sharp JH (2001) The microstructure and mechanical properties of blended cements hydrated at various temperatures. Cem Concr Res 31(5):695–702
54. EuroSoilStab (2010) Design guide: Soft soil stabilization. Development of design and construction methods to stabilize soft organic soils. IHS BRE Press ISBN-1860815995
55. Fasihnikoutalab MH, Pourakbar S, Ball RJ, Unluer C, Cristelo N (2020) Sustainable soil stabilisation with ground granulated blast-furnace slag activated by olivine and sodium hydroxide. Acta Geotech 15:1981–1991. https://doi.org/10.1007/s11440-019-00884-w
56. Fernández-Jiménez A, Puertas I, Sobrados SJ (2003) Structure of calcium silicate crucial insights on the mix design of alkali-activated cement-based binders hydrates formed in alkaline-activated slag: Influence of the type of alkaline activator. J Am Ceram Soc 86(8):1389–1394
57. Fernández-Jiménez A, Palomo A, Criado M (2006) Alkali activated fly ash binders: a comparative study between sodium and potassium activators. Mater Construcc 56:51–65
58. Firat S, Khatib JM, Yilmaz G, Comert AT (2017) Effect of curing time on selected properties of soil stabilized with fly ash, marble dust and waste sand for road sub-base materials. Waste Manage Res. https://doi.org/10.1177/0734242X17705726
59. Forsman J, Jyrävä H, Lahtinen P, Niemelin T, Hyvönen I (2015) Mass stabilization manual. Finland
60. Fournier M, Geoffray J-M (1978) Le Liant pouzzolanes-chaux. Bulletin de Liaison des Laboratoires des Ponts et Chaussees No 93:70–78
61. Franus W, Panek R, Wdowin M (2015) SEM Investigation of Microstructures in Hydration Products of Portland Cement. In:

2nd International multidisciplinary microscopy and microanalysis congress, pp 105–112
62. Galuppo MV (2020) Estudo do emprego da escória granulada de alto-forno na massa de cerâmica de revestimento (in portuguese). Dissertação (Mestrado) Instituto Federal do Espírito Santo Brazil
63. Garcia-Lodeiro I, Fernández-Jimenez A, Palomo A (2015) Cements with a low clinker content: versatile use of raw materials. J Sustain Cem Based Mater 4(2):140–151. https://doi.org/10.1080/21650373.2015.1040865
64. Ghosh A, Ransinchung GD (2022) Application of machine learning algorithm to assess the efficacy of varying industrial wastes and curing methods on strength development of geopolymer concrete. Constr Build Mater 341:127828. https://doi.org/10.1016/j.conbuildmat.2022.127828
65. Gonzalez J, Sargent P, Ennis C (2021) Sewage treatment sludge biochar activated blast furnace slag as a low carbon binder for soft soil stabilisation. J Clean Prod 311:127553. https://doi.org/10.1016/j.jclepro.2021.127553
66. Gurgel GHM (2020) Efeito da incorporação da nanossílica em pastas de cimento com alto teor de fíler calcário (in portuguese). Dissertação (Mestrado) Universidade de Brasília Brazil
67. Gutiérrez HP, de La Vara RS (2012) Análisis y diseño de experimentos. 3ªedn. McGraw-Hill Educación, México
68. Hakkinen T (1993) The influence of slag content on the microstructure, permeability and mechanical properties of concrete. Part 1: microstructural studies and basic mechanical properties. Cem Concr Res 23:407–421
69. Head KH (2006) Manual of soil laboratory testing. Volume 1: Soil Classification and Compaction Tests. 3th edn. Whittles Publishing Scotland UK
70. Horpibulsuk S, Phetchuay C, Chinkulkijniwat A (2012) Soil stabilization by carbide residue and fly ash. J Mater Civ Eng 24(2):184–193
71. ICSD (Inorganic Crystal Structure Database) (2022). ICSD for http://icsd.fiz-karlsruhe.de. Accessed October 08 2022
72. Jendrysik K, Jończyk M, Kanty P (2021) Mass stabilization as a modern method of substrate strengthening. Mater Today Proc 38(4):2068–2072. https://doi.org/10.1016/j.matpr.2020.10.143
73. Jennings HM (2000) A model for the microstructure of calcium silicate hydrate in cement paste. Cem Concr Res 30:101–116. https://doi.org/10.1016/S0008-8846(99)00209-4
74. Jung W, Choi S-J (2017) Effect of high-temperature curing methods on the compressive strength development of concrete containing high volumes of ground granulated blast-furnace slag. Adv Mater Sci Eng
75. Karlsson R, Hansbo S (1989) Soil Classification and Identification. Swedish Council for Building Research Document D8 Stockholm Sweden, p 52
76. Khanday SA, Hussain M, Das AK (2021) A Review on Chemical Stabilization of Peat. Geotech Geol Eng 39:5429–5443. https://doi.org/10.1007/s10706-021-01857-1
77. Kinuthia J, Wild S (1998) Soil stabilisation using lime activated GGBS. Sixth CANMET/ACI/JCI–International Conference Fly ash, Silica Fume, Slag and natural Pozzolans in concrete, Vol 2
78. Kitazume M, Terashi M (2013) The deep mixing method. CRC Press Taylor and Francis group
79. Klug HP, Alexander LE (1974) X-ray diffraction procedures. 2nd edn. John Wiley and Sons Inc, New York, p 996
80. Kourti I, Amutha Rani D, Boccaccini AR, Cheeseman CR (2011) Geopolymers from DC plasma–treated air pollution control residues, metakaolin, and granulated blast furnace slag. J Mater Civ Eng 23(6):735–740. https://doi.org/10.1061/%28ASCE%29MT.1943-5533.0000170
81. Kunal; Siddique R, Rajor A, Singh M (2016) Influence of bacterial-treated cement kiln dust on strength and permeability of concrete. J Mater Civ Eng 28(10): 04016088. https://doi.org/10.1061/%28ASCE%29MT.1943-5533.0001593
82. Lang L, Chen B, Li N (2020) Utilization of lime/carbide slag-activated ground granulated blast-furnace slag for dredged sludge stabilization. Mar Georesour Geotechnol. https://doi.org/10.1080/1064119X.2020.1741050
83. Lemos SGFP, Almeida MSS, Consoli NC, Nascimento TZ, Polido UF (2020) Field and laboratory investigation of highly organic clay stabilized with Portland cement. J Mater Civ Eng 32(4):04020063. https://doi.org/10.1061/(asce)mt.1943-5533.0003111
84. Liu Y, Fu S, Gao J, Yang Y (2020) Prediction for temperature evolution and compressive strength of non-mass concrete with thermal insulation curing in cold weather. J Build Eng 32:101737. https://doi.org/10.1016/j.jobe.2020.101737
85. Lotero A, Consoli NC, Moncaleano CJ, Tebechrani Neto A, Koester E (2021) Mechanical properties of alkali-activated ground waste glass-carbide lime blends for geotechnical uses. J Mater Civ Eng. https://doi.org/10.1061/(ASCE)MT.1943-5533.0003918
86. Lotero A, Consoli NC, Moncaleano CJ (2023) Alkali-activated red ceramic wastes-carbide lime blend: An alternative alkaline cement manufactured at room temperature. J Build Eng 65:105663. https://doi.org/10.1016/j.jobe.2022.105663
87. Maciel MH (2017) Influência do ligante pré-hidratado nas propriedades de suspensões de cimento Portland (in portuguese). Dissertação (Mestrado) Escola Politécnica da Universidade de São Paulo Brazil
88. Moayedi H, Nazir R (2018) Malaysian Experiences of Peat Stabilization, State of the Art. Geotech Geol Eng 36:1–11. https://doi.org/10.1007/s10706-017-0321-x
89. Montgomery DC (2009) Introduction to statistical quality control. 6th edn. John Wiley & Sons Inc
90. Moreira CC (2006) Características e desempenho da escória de alto forno como agregado para utilização em camadas granulares de pavimento (in portuguese). 37ª Reunião Anual de Pavimentação 11° Encontro Nacional de Conservação Rodoviária 37ª RAPv/11° ENACOR N°103 Goiânia Brazil
91. Najafi E, Allahverdi A (2009) Effects of curing time and temperature on strength development of inorganic polymeric binder based on natural pozzolan. J Mater Sci 44(12):3088–3097. https://doi.org/10.1007/s10853-009-3411-1
92. Nidzam RM, Kinuthia JM (2010) Sustainable soil stabilisation with blast furnace slag–a review. Proc Inst Civ Eng Constr Mater 163:157–165
93. Özbay E, Erfemir M, Durmus HI (2016) Utilization and efficiency of ground granulated blast furnace slag on concrete properties–a review. Constr Build Mater 105:423–434
94. Park S, Baker JO, Himmel ME, Parrilla PA, Johnson DK (2010) Cellulose crystallinity index: measurement techniques and their impact on interpreting cellulase performance. Biotechnol Biofuels 3(1):10
95. Puertas F, Martínez-Ramirez S, Alonso S, Vázquez T (2000) Alkali-activated fly ash/slag cement: strength behaviour and hydration products. Cem Concr Res 30:1625–1632
96. Puertas F, Palacios M, Manzano H, Dolado JS, Rico A, Rodríguez J (2011) A model of the C–S–A–H gel formed in alkali-activated slag cements. J Eur Ceram Soc 31:2043–2056
97. Rispoli C, de Bonis A, Guarino V, Graziano SF, Di Benedetto C, Esposito R, Morra V, Cappelletti P (2019) The ancient pozzolanic mortars of the Thermal complex of Baia (Campi Flegrei, Italy). J Cult Herit. https://doi.org/10.1016/j.culher.2019.05.010
98. Rispoli C, de Bonis A, Esposito R, Graziano SF, Langella A, Mercurio V, Morra V, Cappelletti P (2020) Unveiling the secrets of Roman craftsmanship: mortars from Piscina Mirabilis (Campi

Flegrei, Italy). Archaeol Anthropol Sci. https://doi.org/10.1007/s12520-019-00964-8
99. Rotaru R, Savin M, Tudorachi N, Peptu C, Samoila P, Sacarescu L, Harabagiu V (2018) Ferromagnetic iron oxide–cellulose nanocomposites prepared by ultrasonication. Polym Chem 9(7):860–868. https://doi.org/10.1039/c7py01587a
100. Ruland W (1961) X-ray determination of crystallinity and diffuse disorder scattering. Acta Crystallogr 14:1180–1185. https://doi.org/10.1107/s0365110x61003429
101. Saldanha RB, da Rocha CG, Lotero A, Consoli NC (2021) Technical and environmental performance of eggshell lime for soil stabilization. Constr Build Mater 298:123648
102. Saldanha RB, Scheuermann Filho HC, Mallmann JEC, Consoli NC, Reddy K (2018) Physical-mineralogical-chemical characterization of carbide lime: an environment-friendly chemical additive for soil stabilization. J Mater Civ Eng 30(6):06018004
103. Santos CP, Bruschi GJ, Mattos JRG, Consoli NC (2021) Stabilization of gold mining tailings with alkali-activated carbide lime and sugarcane bagasse Ash. Transp Geotech. https://doi.org/10.1016/j.trgeo.2021.100704
104. Sargent P (2015) The development of alkali-activated mixtures for soil stabilisation. In: Handbook of Alkali-Activated Cements Mortars and Concretes, pp 555–604
105. Sargent P (2021) Greener Ground - using recycled industrial waste in ground engineering. Mater World 29(12):45–47
106. Scrivener K, Snellings R, Lothenbach B (2016) A practical guide to microstructural analysis of cementitious materials. CRC Press Taylor & Francis Group LLC
107. Secco MP, Mesavilla DT, Floss MF, Consoli NC, Miranda T, Cristelo N (2021) Live-scale testing of granular materials stabilized with alkali-activated waste glass and carbide lime. Appl Sci. https://doi.org/10.3390/app112311286
108. Seo J, Park S, Yoon H, Jang J, Kim S, Lee H (2019) Utilization of calcium carbide residue using granulated blast furnace slag. Materials 12:3511. https://doi.org/10.3390/ma12213511
109. Serne R, Westsik Jr J (2011) Data package for secondary waste form down-selection-cast stone. US Department of Energy Pacific Northwest National Laboratory
110. Sharma K, Kumar A (2020) Utilization of industrial waste—based geopolymers as a soil stabilizer-A review. Innov Infrastruct Solut 5:97. https://doi.org/10.1007/s41062-020-00350-7
111. Shi C, Day RL (1993) Chemical activation of blended cements made with lime and natural pozzolans. Cem Concr Res 23(6):1389–1396
112. Shenbagam VK, Rolands Cepuritis R, Chaunsali P (2021) Influence of exposure conditions on expansion characteristics of lime-rich calcium sulfoaluminate-belite blended cement. Cem Concrete Compos 118:103932. https://doi.org/10.1016/j.cemconcomp.2021.103932
113. Song S, Sohn D, Jennings HM, Mason TO (2000) Hydration of alkali-activated ground granulated blast furnace slag. J Mater Sci 35:249–257
114. Taylor HFW (1993) Nanostructure of C-S-H: Current status. Adv Cem Based Mater 1:38–46
115. Taylor JC, Aldridge LP (1993) Full-profile Rietveld quantitative XRD analysis of Portland cement: Standard XRD profiles for the major phase tricalcium silicate (C3S: $3CaO{\cdot}SiO_2$). Powder Diffr 8(3):138–144. https://doi.org/10.1017/s0885715600018054
116. Thomé A (1999) Comportamento de fundações superficiais apoiadas em aterros estabilizados com resíduos industriais (in portuguese). Tese (doutorado)–UFRGS–Programa de Pós-Graduação em Engenharia Civil Brazil
117. Thygesen A, Oddershede J, Lilholt H, Thomsen AB, Ståhl K (2005) On the determination of crystallinity and cellulose content in plant fibres. Cellulose 12(6):563–576. https://doi.org/10.1007/s10570-005-9001-8)
118. Trindade AC, Alcamand HA, Borges PH, Silva FA (2017) On the durability behavior of natural fiber reinforced geopolymers. In: 41st international conference and expo on advanced ceramics composites
119. Torres-Carrasco M, Puertas F (2017) Alkaline activation of different aluminosilicates as an alternative to Portland cement: Alkali activated cements or geopolymers. Revista Ingeniería de Construcción 32(2):5–12
120. Vichan S, Rachan R (2013) Chemical stabilization of soft Bangkok clay using blend of calcium carbide residue and biomass ash. Soils Found 53(2):272–281
121. Vonk CG (1973) Computerization of Rulands X-ray method for determination of crystallinity in polymers. J Appl Crystallogr 6:148–152
122. Wang DX, Zentar ZR, Abriak NE (2017) Temperature-accelerated strength development in stabilized marine soils as road construction materials. J Mater Civ Eng. https://doi.org/10.1061/%28ASCE%29MT.1943-5533.0001778
123. Wheeler LN, Take WA, Neil A (2017) Hoult. Performance assessment of peat rail subgrade before and after mass stabilization. Can Geotech J 54(5):674–689. https://doi.org/10.1139/cgj-2016-0256
124. Yi Y, Gu L, Liu S, Puppala AJ (2015) Carbide slag–activated ground granulated blast furnace slag for soft clay stabilization. Can Geotech J 52(5):656–663. https://doi.org/10.1139/cgj-2014-0007
125. Yulianto FE, Basuki W (2019) Modelling of crystal growth in peat soil stabilized with mixing of lime $CaCO_3$ and fly ash. Int J Civ Eng Technol 10(3):49–360